NRC FORM 335 (2.84) NRCM 1102, 3201, 3202

U.S. NUCLEAR REGULATORY COMMISSION

BIBLIOGRAPHIC DATA SHEET

SEE INSTRUCTIONS ON THE REVERSE

1. REPORT NUMBER (Assigned by TIDC, add Vol. No., if any)
NUREG/CR-4137
SAND85-0175

2. TITLE AND SUBTITLE
Pretest Predictions for the Response of a 1:8-Scale Steel LWR Containment Building Model to Static Overpressurization

3. LEAVE BLANK

4. DATE REPORT COMPLETED
MONTH: June
YEAR: 1985

5. AUTHOR(S)
David B. Clauss

6. DATE REPORT ISSUED
MONTH: July
YEAR: 1985

7. PERFORMING ORGANIZATION NAME AND MAILING ADDRESS (Include Zip Code)
Sandia National Laboratories
Albuquerque, NM 87185

8. PROJECT/TASK/WORK UNIT NUMBER

9. FIN OR GRANT NUMBER
A1401

10. SPONSORING ORGANIZATION NAME AND MAILING ADDRESS (Include Zip Code)
Division of Engineering Technology
Office of Nuclear Regulatory Research
U. S. Nuclear Regulatory Commission
Washington, DC 20555

11a. TYPE OF REPORT

b. PERIOD COVERED (Inclusive dates)

12. SUPPLEMENTARY NOTES

13. ABSTRACT (200 words or less)

The analyses used to predict the behavior of a 1:8-scale model of a steel LWR containment building to static overpressurization are described and results are presented. Finite strain, large displacement, and nonlinear material properties were accounted for using finite element methods. Three-dimensional models were needed to analyze the penetrations, which included operable equipment hatches, personnel lock representations, and a constrained pipe. It was concluded that the scale model would fail due to leakage caused by large deformations of the equipment hatch sleeves.

14. DOCUMENT ANALYSIS - a. KEYWORDS/DESCRIPTORS
containment building
overpressurization
severe accidents

15. AVAILABILITY STATEMENT
Unlimited

16. SECURITY CLASSIFICATION
(This page)
Unclassified
(This report)

b. IDENTIFIERS/OPEN-ENDED TERMS

17. NUMBER OF PAGES

18. PRICE

NUREG/CR–4137
SAND85–0175
R1, RD
Printed June 1985

Pretest Predictions for the Response of a 1:8-Scale Steel LWR Containment Building Model to Static Overpressurization

David B. Clauss

Prepared by
Sandia National Laboratories
Albuquerque, New Mexico 87185 and Livermore, California 94550
for the United States Department of Energy
under Contract DE-AC04-76DP00789

Prepared for
U. S. NUCLEAR REGULATORY COMMISSION

Available from

Superintendent of Documents
U.S. Government Printing Office
Post Office Box 37082
Washington, D.C. 20013-7982

and

National Technical Information Service
Springfield, VA 22161

NUREG/CR-4137
SAND85-0175
R1,RD

PRETEST PREDICTIONS FOR THE RESPONSE OF A 1:8-SCALE STEEL LWR CONTAINMENT BUILDING MODEL TO STATIC OVERPRESSURIZATION

David B. Clauss

June 1985

Sandia National Laboratories
Albuquerque, NM 87185
Operated by
Sandia Corporation
for the
U.S. Department of Energy

Prepared for
Mechanical/Structural Engineering Branch
Division of Engineering Technology
Office of Nuclear Regulatory Research
US Nuclear Regulatory Commission
Washington, DC
Under Memorandum of Understanding DOE 40-550-75
NRC FIN No. A1401

ABSTRACT

The analyses used to predict the behavior of a 1:8-scale model of a steel LWR containment building to static overpressurization are described and results are presented. Finite strain, large displacement, and nonlinear material properties were accounted for using finite element methods. Three-dimensional models were needed to analyze the penetrations, which included operable equipment hatches, personnel lock representations, and a constrained pipe. It was concluded that the scale model would fail due to leakage caused by large deformations of the equipment hatch sleeves.

CONTENTS

FIGURES AND TABLES

FIGURES AND TABLES

ACKNOWLEDGMENT

Thanks are due Dan Horschel and Tom Blejwas, both of the Containment Integrity Division. Their pioneering work on the 1:32-scale steel models paved the way for the analyses of the 1:8-scale model. In addition, Dan kept MARC up and running (usually), and always seemed to have a ready answer for my questions about MARC. Tom Blejwas provided many valuable insights and suggestions. Thanks also to Gerry Knorowsky of the Process Metallurgy Division for his efforts in evaluating the material properties.

1. EXECUTIVE SUMMARY

Sandia National Laboratories is conducting scale model experiments of nuclear containment buildings subject to static overpressurization. The objective of the experiments is to generate data that can be used to qualify methods for reliably predicting the response of containment buildings during severe accidents. This report documents the pretest calculations for the 1:8-scale steel containment model, which was pressurized to failure in November 1984. The pretest predictions were used in planning the type and location of instrumentation, and the conduct of the high pressure test. In addition, analyses conducted prior to the test cannot be biased by experimental results, and therefore a more accurate assessment of analytical capabilities can be obtained.

The 1:8-scale model was designed for 40 psig by Chicago Bridge and Iron Company following ASME pressure vessel code standards. The model, which was fabricated from A516 Gr70 steel, consisted of a 3/16 inch thick cylindrical shell that was welded to a hemispherical dome. The cylinder was roughly 14.5 feet in length, with a diameter of 14 feet. Circumferential stiffening rings were attached to the external surface of the cylinder at 15 inch intervals. There were a total of eleven penetrations that passed through the cylinder, including two operable equipment hatches, two personnel lock representations, and seven pipe penetrations. 'O' rings were used to form a seal between the equipment hatch sleeves and covers. Two 'constrained' pipe penetrations passed through the cylinder at diametrically opposed points, and were connected to each other by an integral length of pipe. The cylinder was reinforced at all penetrations as required by ASME code. Details of the design and fabrication of the 1:8-scale model are available in [7].

Finite element methods were used to analyze the response of the model subject to static overpressurization. Thin shell elements were used to model the structure, and large displacement, finite strain, and nonlinear material behavior were taken into account. The Von Mises yield criterion was used with full Newton Raphson iteration. Rupture was assumed to occur if the equivalent membrane strain exceeded 15%, or if the equivalent bending strain exceeded 20% at any point. Leakage was expected when a total mismatch of the sealing surfaces occurred.

Predictions for the response of the 1:8-scale model to static overpressurization were based on five separate analyses, each of which covered a different area of the structure. An axisymmetric model of the ring stiffened shell (no penetrations) was used to predict strains and displacements in the hemispherical head, and in the cylinder near its attachment to the fixturing. The response of the equipment hatch covers was also evaluated using an axisymmetric model. The response of each of the major penetrations (the constrained pipe, both equipment hatches, and personnel lock 2) and of the cylinder due to its

interaction with these penetrations was determined using three separate three-dimensional models.

Initial yielding occurred in areas characterized by bending behavior, such as the equipment hatch sleeves near their intersection with the cylindrical wall, and the cylinder at its attachment to the fixturing. First yield occurred at 52 psig. However, bending strains did not increase rapidly until after membrane yielding of the cylinder began. The predicted membrane yield pressure was 180 psig; however, the actual value was expected to be 5 to 15 percent lower because of changes in the material properties associated with fabrication and strain rate effects.

Strain concentrations were predicted in the cylinder adjacent to the reinforcement around penetrations. The severity of a strain concentration depended on the combined stiffness of the reinforcement and penetration. These strain concentrations reduced the strength of the model relative to a model with no penetrations. Although the constrained pipe penetrations prevented radial expansion of the cylinder at their intersection, they had little or no effect on the model's strength. There was no evidence of significant interaction between penetrations.

The model was expected to fail by 210 psig due to excessive leakage caused by large distortions of the equipment hatch sleeve. The equipment hatch sleeve deformed into an oval shape, with the displacement increasing rapidly as the pressure was increased beyond the membrane yield pressure. The strains in the model at 210 psig were well below the maximum strains permitted by the rupture criterion.

Comparisons between predictions and experiments, and an assessment of analytical capabilities will be made available in a soon to be published report [6].

2. INTRODUCTION

The Containment Integrity Division at Sandia National Laboratories is testing scale models of containment buildings to determine their response to static, internal pressurization. The models are pressurized to failure using nitrogen gas. To date, four 1:32-scale steel models and a 1:8-scale steel model have been tested. Analyses were conducted prior to these tests to obtain unbiased predictions for the models' response, and also to help plan instrumentation. A complete description of the fabrication, analyses, and testing of the 1:32-scale models is available in [1]. This report will describe the analyses used to predict the response of the 1:8-scale model.

The scale model tests are one of a series of NRC-funded programs that are investigating containment integrity during severe accidents [2]. The containment building is the last engineered barrier preventing the release of radioactive materials. During a severe accident, the pressure and temperature inside the containment could significantly exceed the design basis loads. The capacity of the containment building and the timing, mode and location of a failure affect the consequences and risks associated with a severe accident. The containment should theoretically be capable of withstanding pressures and temperatures beyond the design basis since the design is based on linear, elastic behavior with large factors of safety. The containment's ability to strain and deform plastically is not explicitly considered during the design process.

The objective of the scale model tests is to generate a structural data base that can be used to qualify methods for predicting the structural behavior of containments, particularly the nonlinear response. The scale models were designed and fabricated in a manner as representative of actual containments as possible, given the restrictions imposed by the size reduction. The features of the 1:8-scale model are more representative of actual containments than those of the 1:32-scale models.

Testing of the 1:8-scale steel containment model was successfully conducted November 15-17, 1984. The model ruptured after the pressure was increased to 195 psig. Nearly 1000 channels of data, including strain, displacement, and leak rate measurements, were recorded at 21 different pressure levels. Details of the conduct of the test and the test results are reported in [3] and [4]. Comparisons of test data with analytical results suggests that strains and displacements in steel containments can be predicted with reasonable accuracy, but additional effort is needed to develop failure criteria. Additional details on the assessment of predictive capabilities are available in [5] and [6].

3. DESCRIPTION OF THE MODEL

Chicago Bridge and Iron Company designed the model, fabricated it in Salt Lake City, transported it, and erected the model on site in Albuquerque. The important structural features of the model are presented in this section. A complete description of the design, fabrication, as built geometry, and measured material properties of the model are presented in [7].

3.1 Geometry

The 1:8-scale model was built to ASME code specifications with a design pressure of 40 psig. A schematic of the model is shown in Figure 1. The base was a 1-3/16 inch thick ellipsoidal shell that was used as a test fixture. The base was very stiff relative to the model, and consequently it served as a convenient reference for measuring displacements. The model consisted of a cylindrical shell that was welded to a hemispherical dome. The cylinder was 172.5 inches in length, and had an 84 inch radius. The nominal thickness of the cylinder and dome was 3/16 inch; however, the average thicknesses of the plates used to fabricate the cylinder and dome were 0.197 inch and 0.205 inch, respectively. Eight thickness measurements were made on each plate, and the measured thickness of the six plates used to fabricate the cylinder ranged from 0.186 inch to 0.227 inch. Only the nominal thickness will be reported from here on; the actual average plate thickness and the range of measurements, as well as where the plates were used can be determined from Table 1. Circumferential stiffening rings were attached to the external surface of the cylinder at 15 inch intervals, beginning 6 inches above the cylinder to base weldment (lower springline). These rings were 2-3/4 inch wide by 3/16 inch thick. Each ring was supported by gussets spaced roughly 12° apart in the circumferential direction.

Eleven penetrations passed through the cylinder including seven pipe penetrations, two personnel lock representations, and two operable equipment hatches. The cylinder was reinforced at all penetrations as required by the ASME code. The nominal thickness of the reinforcement was 3/8 inch, except the reinforcement for the equipment hatches, which was 1/2 inch. The locations of the penetrations are shown in Figure 2. The five "unconstrained" pipe penetrations, SA, SB, SC, SD, and SE, were comprised of standard size seamless pipe with a flat cover welded to the end of the pipe inside the cylinder. The 'constrained' pipe penetrations, SF1 and SF2, passed through the cylinder at diametrically opposed points and were connected to each other by an integral length of pipe. SF1, SF2, and the connecting pipe were 8"ϕ Sch 40 seamless pipe, which has an outside diameter of 8.62 inch and a thickness of 0.32 inch. Flat covers, which were 1-1/8" thick, were welded to the ends of SF1 and SF2 outside the model. The two personnel lock representations, PL1 and PL2, were comprised of 12"ϕ XSTG seamless pipe with flat covers welded to both ends. The pipe was machined so that the final thickness was 3/8 inch at the intersection with the cylinder, and 3/16 inch

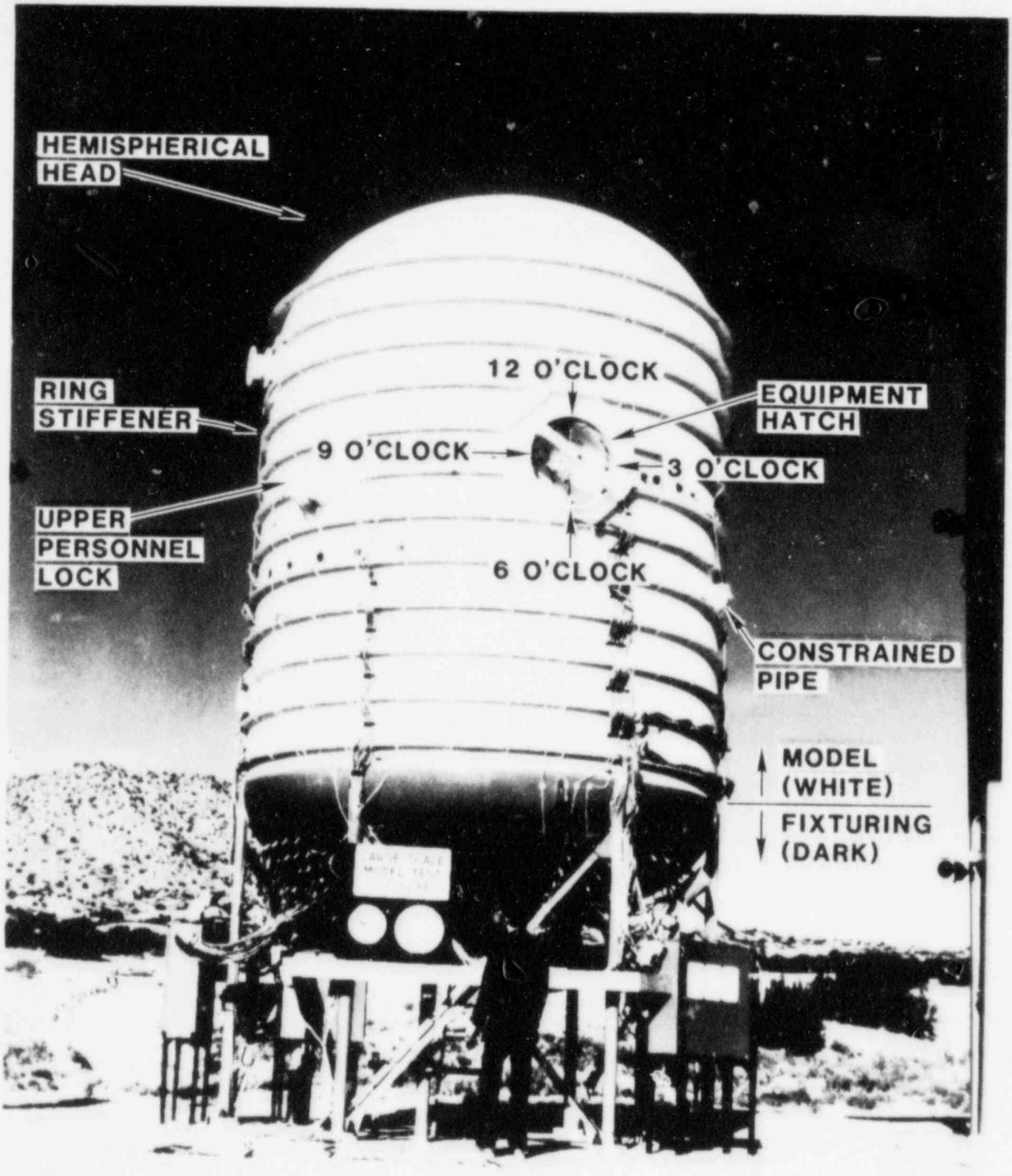

Figure 1 1:8-Scale Steel Containment Model

Table 1

PLATE MATERIALS IN THE 1:8-SCALE MODEL

Nominal Thickness	No. of Plates	Average Thickness	Range of Measurements	Use of Plates in Model
3/16"	6	0.197"	0.186"-0.227"	Cylinder
3/16"	7	0.205"	0.194"-0.220"	Hemispherical Dome and Ring stiffeners
3/8"	1	0.394"	0.382"-0.410"	Reinforcement for SA, SB, SC, SD, SE, SF1, SF2, PL1, and PL2, Inside Covers for PL1 and PL2, Spherical Covers for EH1 and EH2
1/2"	1	0.505"	0.497"-0.510"	Reinforcement for EH1 and EH2
1-1/8"	1	1.161"	1.153"-1.168"	Sleeves for EH1 and EH2, Outside covers for PL1 and PL2
1-3/16"	2	1.211"	1.200"-1.225"	Ellipsoidal base
1-1/2"	1	1.531"	1.525"-1.540"	Dish for base, Covers for SA, SB, SC, SD, and SE
1-5/8"	1	1.682"	1.669"-1.690"	Covers for SF1 and SF2

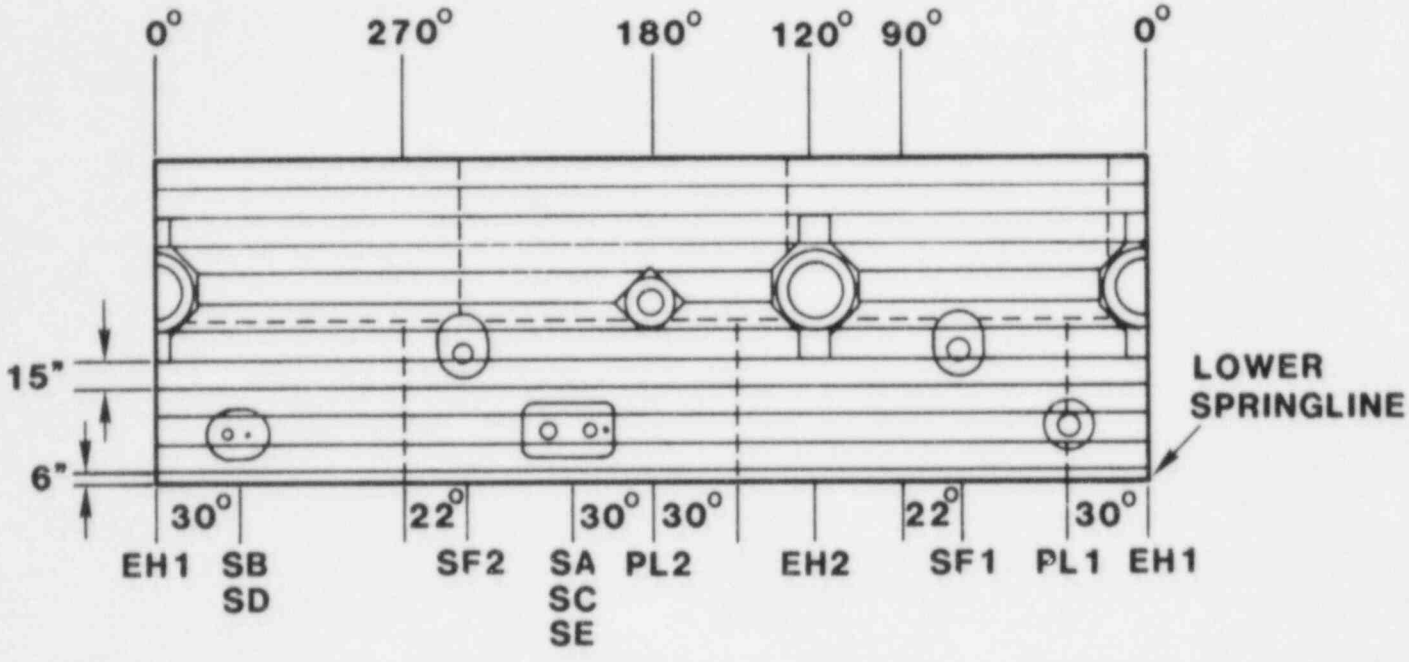

Figure 2 Cylinder Stretchout

away from it, as shown in Figure 3. The equipment hatches, EH1 and EH2, were located at the same elevation, but 120° apart. The sleeves were welded into a cylindrical shape from plate with a nominal thickness of 1-1/8 inch before machining. The final cross sectional shape of the sleeve is shown in Figure 4. An "O" ring was used to provide a seal between the sleeve and the cover tensioning ring. The cover itself was formed from 3/8" plate stock into a 30 inch radius spherical dish.

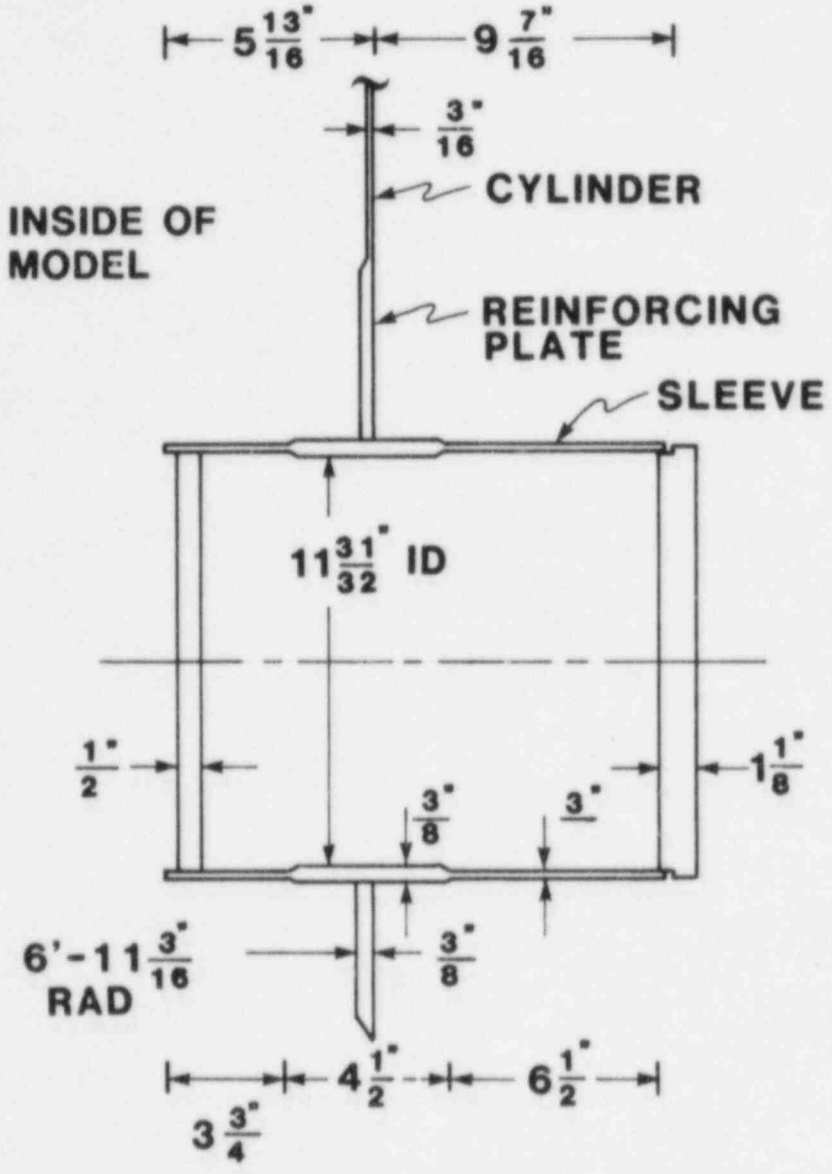

Figure 3 Personnel Lock Representation

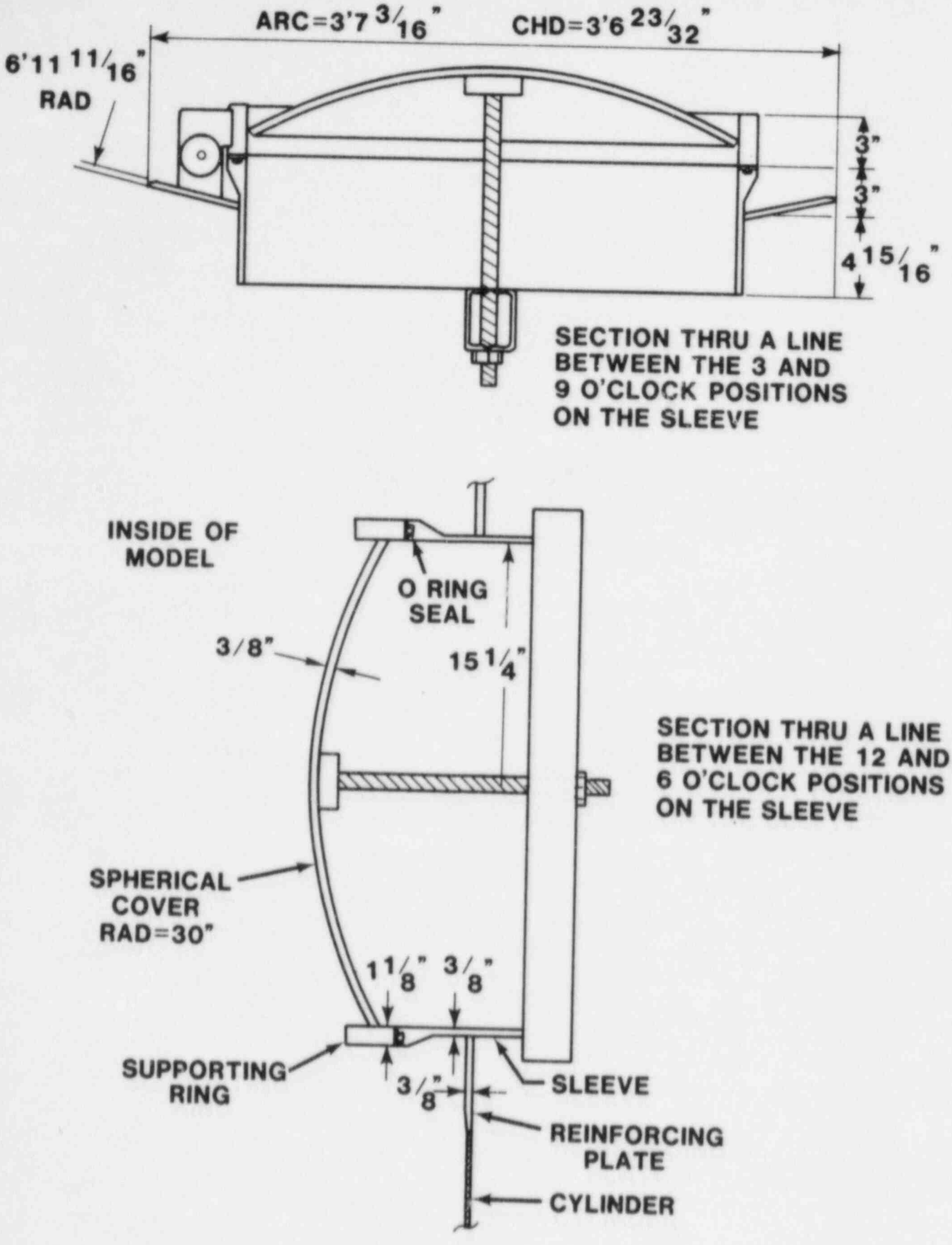

Figure 4 Equipment Hatch

3.2 Material Properties

The 1:8-scale model was fabricated from A516 Gr70 steel, which is frequently used in actual containments. Pipe materials used in the model have a slightly different composition than A516, however, they exhibit approximately the same mechanical properties. A516 steel is a medium carbon steel, intended for low to moderate temperature service, with good hardenability and ductility. The Process Metallurgy Division at Sandia conducted numerous mechanical and physical tests to determine true stress-true strain curves, Young's modulus, shear modulus, and Poisson's ratio for the actual construction materials. Details of the mechanical testing can be found in Appendix C of [7]. Raw material for test specimens came from remnants or cutouts for penetrations. The only materials not tested were the seamless pipe for penetrations SA, SB, SC, SD, and SE and the bottom dollar plate for the base. These materials were not expected to be highly stressed, and therefore no need existed for detailed properties.

Elastic constants were determined using ultrasonic methods. Almost no variation in the elastic constants was detected for the various specimens tested. In the analyses, Young's modulus, the shear modulus, and Poisson's ratio were input as 30.68 Mpsi, 11.93 Mpsi, and 0.286, respectively, for all materials.

The true stress-true strain curves used in the analyses are shown in Figure 5. Engineering stress-strain curves were recorded from fairly standard uniaxial tensile tests. Engineering curves were then converted to true stress-true strain curves using the well known equations

$$\sigma_T = \sigma_E(1 + \varepsilon_E)$$

$$\varepsilon_T = \ln(1 + \varepsilon_E),$$

which are valid up to the point of maximum load. For the materials tested, the strain at maximum load varied from 0.15 to 0.18, and the fracture strain was from 0.32 to 0.47.

4. ANALYTICAL METHODS AND PROCEDURES

4.1 Finite Element Techniques

Analyses of the 1:8-scale model was conducted using the K.1 version of MARC, a general purpose finite element code [8]. Options that account for finite strain, large displacement, and nonlinear material behavior were selected. Thin shell elements were used to represent the structure. For three-dimensional analysis, PATRAN-G [9] was used to generate the mesh, assign thickness and material properties to the elements, and apply boundary conditions and initial load increments. Subsequent load increments were defined manually using the proportional increment

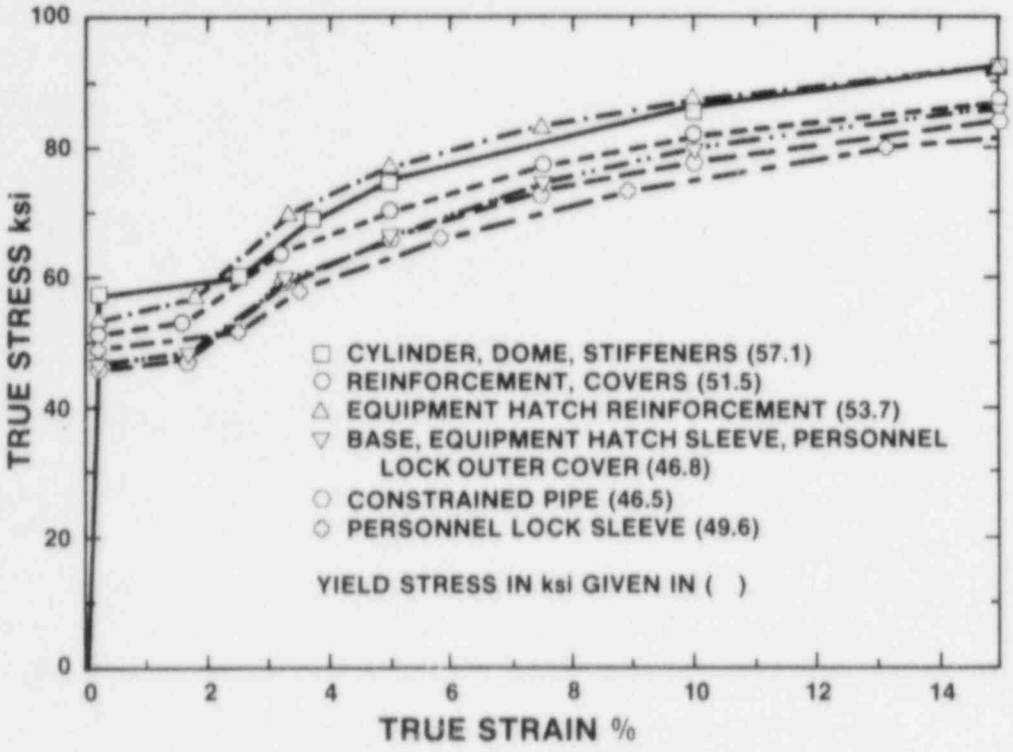

Figure 5 True Stress-True Strain Curves for Model Materials

option. Pressure increments of 10 to 25 psi were taken initially; just before membrane yielding the increments were decreased to 1 to 2 psi; finally, increments of 4 to 5 psig were taken once the material began to show significant work hardening (beyond the yield plateau). The convergence criteria was that the maximum allowable value of maximum residual force divided by the maximum reaction force be less than 0.05 (the default is 0.10). MARC uses full Newton-Raphson iteration with a Von Mises yield criteria.

For the three-dimensional analyses, strain contours and deformed shapes were plotted using the post-processing capabilities of PATRAN-G. The contour plots are best considered as qualitative measures of the strain distribution because there is some loss of accuracy involved with the nodal averaging process. For the axisymmetric analyses, deformed shapes were produced with the plotting capabilities of MARC. Spatial plots, which show the distribution of strain or displacement for a fixed meridional or circumferential location at a given pressure, and pressure history plots, which show the strain or displacement as a function of pressure for a given location, were produced using a code written by the author. This code reads the results file from MARC, and interactively queries the user to define the plot. The code has capabilities to extrapolate element values to nodal locations, and to interpolate nodal values to any coordinates the user selects. This feature enabled direct comparison of analytical and experimental results [6], since pressure histories could

be plotted at the physical location of the instrumentation. The MARC post tape and restart tape were saved on magnetic tape for all analyses. Input card file images and analysis files were also saved.

Only the penetrations near midheight of the cylinder were specifically analyzed. The "unconstrained" pipe penetrations and PL1 were in an area of low membrane strains and deformation due to the constraint imposed by the ellipsoidal base on the cylinder, and were therefore not expected to have nearly as important an effect on the model's response as that of the penetrations near midheight. Also the pipe penetrations were very stiff, so that a sleeve failure (due to bending strains, for instance) was considered unlikely. Welds were not modeled. Preliminary analyses of the 1:8-scale model were reported in [10] and [11] and internal memorandums. These analyses used the geometry as specified on the drawings and a bilinear stress-strain curve based on the yield stress and ultimate stress and strain reported by the mill. The results of these analyses were used to plan the instrumentation, and also led to a number of improvements in the finite element models used in the final analyses. Comparisons of analyses of a clean shell to a ring stiffened shell indicated that the effect of stiffeners on the membrane response could be modeled implicitly, by increasing the thickness of the cylinder by an amount which accounts for the volume of the stiffeners. However, explicit modeling of the stiffeners around the equipment hatch resulted in smaller deformations and lower bending strains in the sleeve than with the stiffeners implicitly modeled, which showed that stiffeners could have important local effects that could not be modeled using simple techniques. The preliminary analyses also demonstrated that the flat plate covers that are used on all penetrations except the equipment hatches have the same effect on the sleeve as a rigid plug. Therefore, the ends of the personnel lock sleeve and the constrained pipe were not allowed to deform in the analyses presented here. The base was shown to be effectively rigid, so that the cylinder was fixed at the lower springline, except for the ring stiffened model, which was used to determine bending strains at the lower springline.

4.2 Failure Criteria

The seals on the two equipment hatches in the 1:8-scale steel model represented a potential leakage path. Because the seal was pressure seating, opening, or gapping of the sealing surfaces was not considered to be a possible failure mode. However, considerable deformation of the equipment hatch sleeve relative to the cover tensioning ring was expected. The leakage criterion that was used to predict the onset of leakage required a complete mismatch of the sealing surfaces: leakage was defined to occur when the change in the radius of the sleeve was equal to the thickness of the sleeve.

The rupture criterion was based on the maximum equivalent strain. It was assumed that the pressure at which a material

failure (crack) initiated was also the pressure at which rupture would occur. The possibility of stable crack growth or arrest was not considered. When the maximum equivalent strain that was calculated with the finite element model exceeded a critical value, rupture was said to occur. This critical value was determined by taking into account the ultimate strain, the fracture strain, and the gage length, and also observations of the 1:32-scale model tests and membrane tests conducted by Goller [12]. Based on these factors, the critical value was estimated to be 15% for global strain (strain over a large gage length), and 20% for localized or bending strains.

4.3 Comments on the Use of Uniaxial Material Properties

The true stress-true strain curves obtained from the uniaxial tensile tests were used in the analyses without major modification. Results of the 1:32-scale model and the work reported by Goller indicated that the measured yield stress for the 1:8-scale model might be as much as 15% below the yield stress determined using the uniaxial stress-strain curves. The limitations of using uniaxial test data to represent the material behavior of the steel containment models are discussed in Appendix C of [7]. Differing strain rates between the uniaxial tests and the model tests, the Bauschinger effect, and difficulties in applying uniaxial data to multiaxial strain states are cited as contributing to the overprediction of yield stress.

The strain rate for the model tests is about two orders of magnitude less than that for the tensile tests, which would account for about a five percent decrease in yield stress. The Bauschinger effect refers to the observation that the tensile (compressive) yield stress for some materials is reduced when the material has been previously yielded in the compressive (tensile) sense. The cylinder materials underwent compressive plastic deformation on the inner surface when the original plates were rolled into the cylindrical shape. Other materials in the 1:8-scale model were also cold worked. Depending on the amount of cold work, which is difficult to determine precisely, the Bauschinger effect could account for an additional five to ten percent reduction in the yield stress.

The low work hardening slope associated with the yield plateau caused some numerical difficulties with models for which the ring stiffeners were modeled implicitly. A plastic instability can occur if the geometric softening exceeds the material work hardening capability. The work hardening slopes were increased and the yield stress nominally reduced (for example the yield stress for the cylinder material was changed from 58.0 ksi to 57.1 ksi) to avoid the numerical problems. The rings actually yield at a slightly higher pressure than the cylinder, which allows the load to be redistributed. Therefore, no instability associated with the yield plateau was expected during testing.

5. SUMMARY OF ANALYTICAL RESULTS

Predictions of the response of the 1:8-scale model to static internal pressurization were based on five separate analyses, each of which covered a different area of the structure. An axisymmetric model of the ring stiffened shell (no penetrations) was used to predict strains and displacements in the hemispherical head, and in the cylinder near the lower springline. The response of the equipment hatch covers was also evaluated using an axisymmetric model. The response of each of the major penetrations (the constrained pipe, both equipment hatches, and the upper personnel lock) and of the cylinder due to its interaction with these penetrations was determined using three separate three-dimensional models.

Initial yielding of the model was caused by localized bending in the equipment hatch sleeves at 6 and 12 o'clock at their intersection with the reinforcement. The maximum strain for any pressure level occurred at this location. First yield was detected at 52 psig. Large localized bending strains occurred at all significant geometric discontinuities, such as intersections of personnel lock sleeves and the cylinder and the lower springline. However, these bending strains did not increase significantly until after membrane yielding of the cylinder wall occurred. The constrained pipe affected strains throughout the cylinder. For all points on the cylinder, the strains predicted using the constrained pipe model were lower than those predicted with the ring stiffened model. Strain concentrations were predicted in the cylinder adjacent to the reinforcement around penetrations at 3 and 9 o'clock. The strain concentration factor (scf) increased as the plastic strain accumulated in the model increased; at 200 psig the scf was 1.38 for the equipment hatches and 1.54 for PL2, by 225 psig, they had increased to 1.74 and 1.55, respectively, and at 250 psig the scf for PL2 was 1.74. Strain concentrations were also predicted in the reinforcements immediately above and below the penetrations, although these were not as severe as those predicted in the cylinder. These strain concentrations are analogous to the elastic strain concentration around a hole in a flat plate with a 2:1 load ratio.

The analyses showed that membrane yielding of the cylinder would occur at 180 psig. Because of difficulties in using uniaxial material properties to predict model response (see Section 3.3), membrane yielding was expected to occur anywhere from 153 psig to 171 psig during the actual test. This is five to fifteen percent below the membrane yield pressure predicted with MARC, the actual amount depending on the degree to which the Bauschinger effect reduces the yield stress.

The model was expected to fail by 210 psig due to excessive leakage caused by large distortions of the equipment hatch sleeve. Significant leakage was expected when the change in the sleeve radius was equal to the sleeve thickness at the sealing surface. (During the test, the model ruptured before this occurred.) The equipment hatch deformed into an oval shape at

the sealing surfaces, with the displacement increasing rapidly as the pressure was increased beyond the membrane yield pressure. The maximum principal strains in the model at 210 psig varied from 3.5% in the membrane regions, to 5% in the cylinder adjacent to the penetrations, to 9% in the equipment hatch sleeve. These strain levels were well below those that were associated with rupture (analytically).

6. AXISYMMETRIC MODELS

An axisymmetric model of the ring stiffened shell (no penetrations) was used to predict strains and displacements in the hemispherical head and in the cylinder at the lower springline. The response of the equipment hatch covers and the tensioning rings was also determined using an axisymmetric model. MARC element 15, which is a two node, axisymmetric, thin shell element with cubic shape functions that is suitable for large displacement and finite strain behavior, was used in the axisymmetric models.

6.1 Ring Stiffened Shell

The finite element mesh used to model the ring stiffened shell is shown in Figure 6. The model consists of 144 elements with 575 degrees of freedom. The mesh discretization at the lower springline was very fine so that the bending response could be accurately determined. The instrumentation ring and the 12 stiffeners were each represented with a single thin shell element. The radial displacement and the rotation of the base and dome were fixed at the axis of symmetry. Axial displacement was fixed at a node on the base corresponding to the approximate location of its attachment to the supporting columns.

The cylinder first yielded at 86 psig on the internal surface at the lower springline. General yielding of the cylinder did not begin until the pressure reached 180 psig. Yielding at the lower springline was associated primarily with meridional bending strains, which decreased rapidly away from the intersection of the cylinder and base, Figure 7. The circumferential component of strain in the cylinder is small at this location because of the radial constraint imposed by the ellipsoidal base. The effects of the fabrication misalignment between the cylinder and the base, and of the weldment at their intersection were not considered. Nevertheless, the analyses should give an accurate picture of the magnitude and the distribution of the bending strains at the lower springline.

The strains in the hemispherical dome remained elastic up to 250 psig, except for a localized area near the intersection of the dome with the cylinder. The ellipsoidal base behaved essentially as a rigid body; the radial displacement and rotation of the instrumentation ring were .099 in, and .0063 rad respectively, at 225 psig. The internal structure (not modeled),

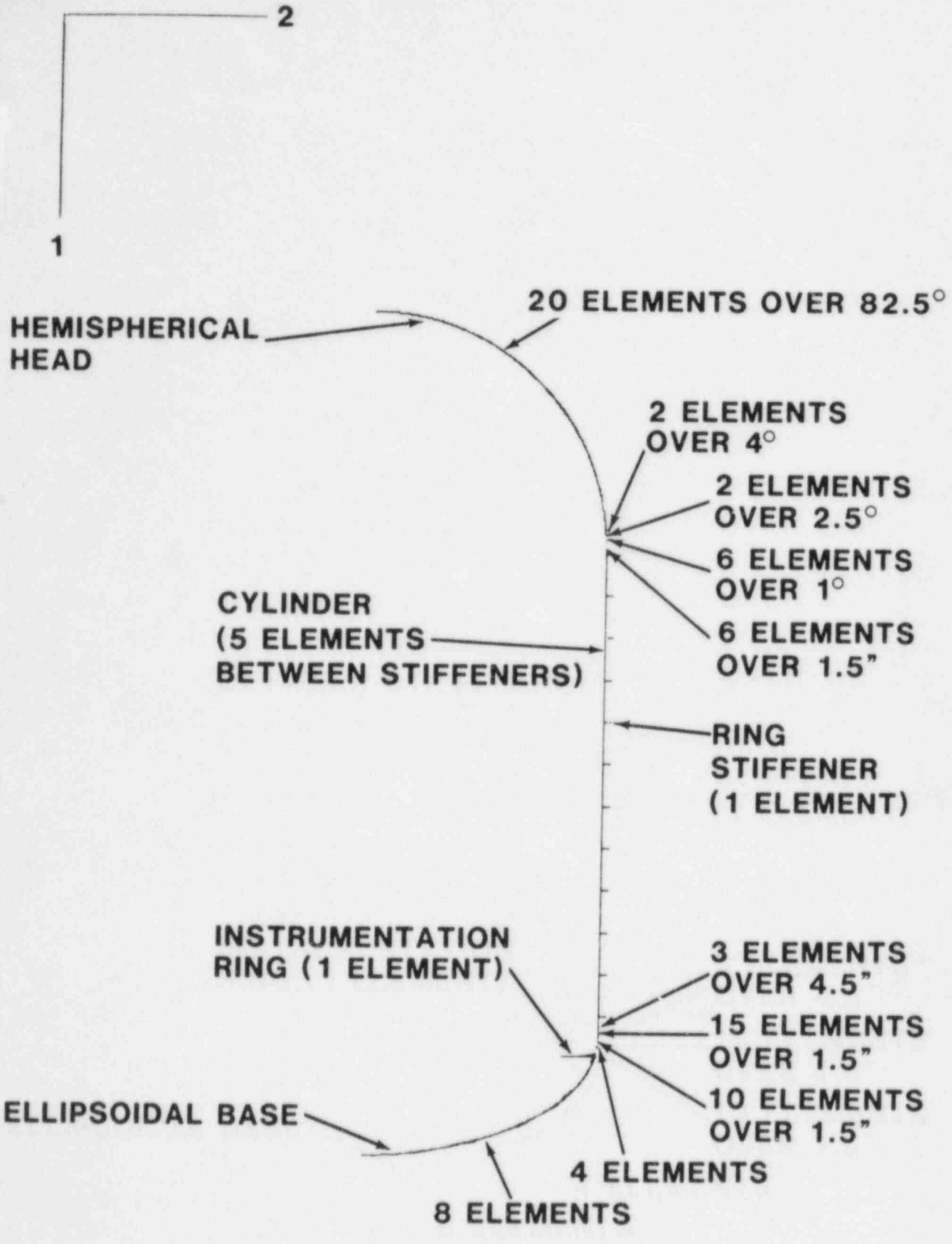

Figure 6 Finite Element Mesh for Ring Stiffened Model

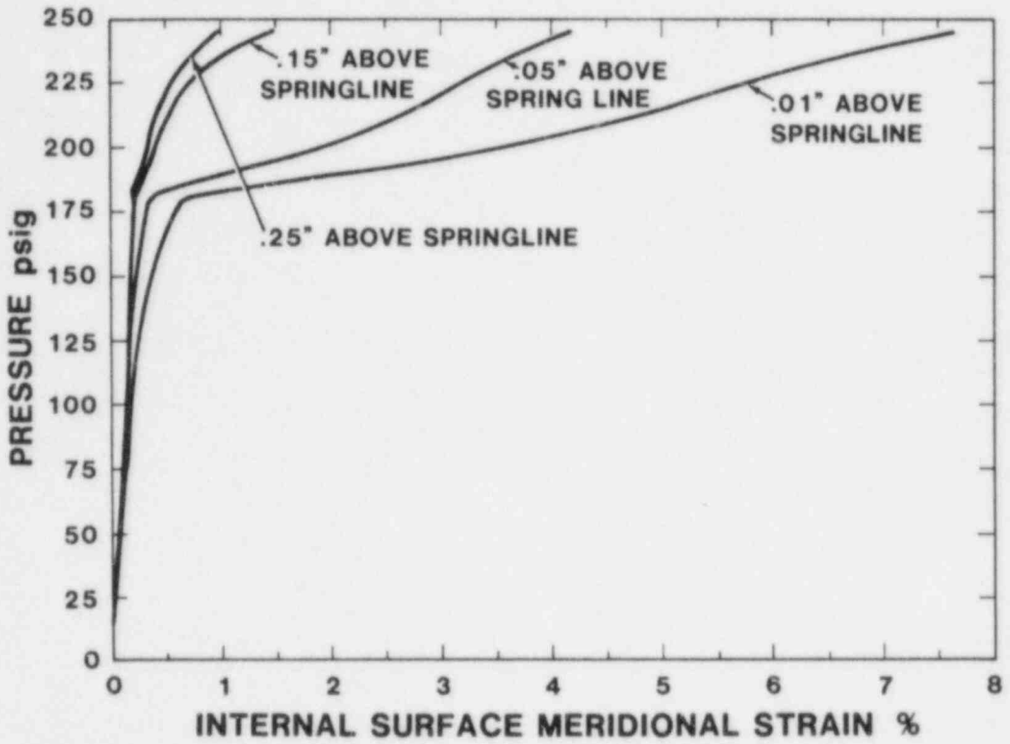

Figure 7 Bending Strains in Cylinder at Lower Springline

which was attached to the instrumentation ring, would tend to resist the rotation of the instrumentation ring (at the top of the cylinder, .0063 rad rotation would necessitate a 1.1" change in radius of the internal structure). As a result, the constraint at the lower springline will probably be greater than what was modeled, and therefore the actual bending strains may be higher than those calculated.

The deformed shape of the model prior to general membrane yielding of the cylinder is shown in Figure 8. In the elastic range, the bulging of the cylinder between stiffeners accounted for a significant portion of the total displacement of the cylinder between stiffeners. However, once the cylinder and the stiffeners began to accumulate plastic strain, their response became more uniform. The deformation of the ring stiffened shell after general yielding occurred, Figure 9, is qualitatively the same as a clean cylinder. The circumferential strain in the stiffeners was slightly less than in the cylinder wall as indicated in Figure 10. Compressive radial strains also were present in the stiffeners, however, the equivalent plastic strain in each ring was less than that in the cylinder at the same elevation.

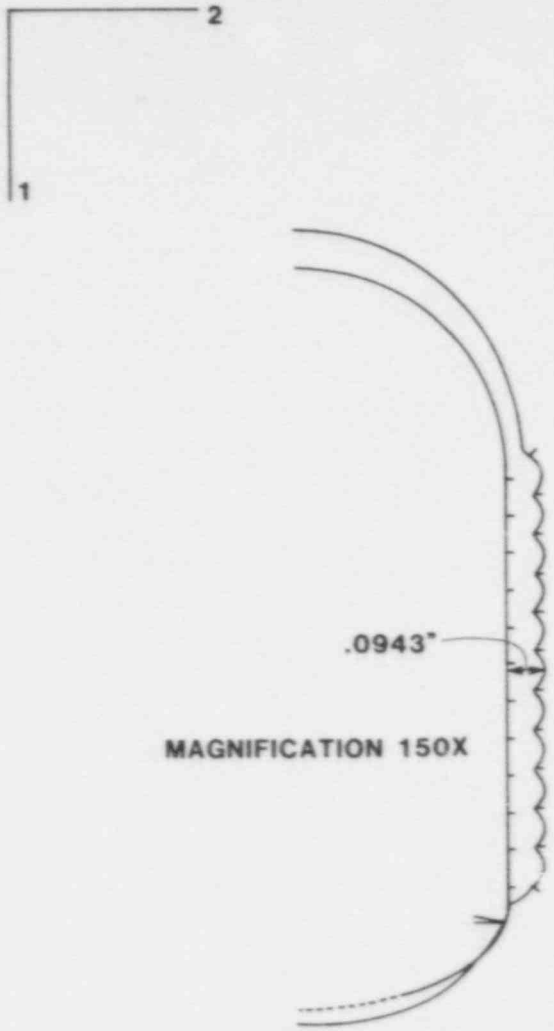

Figure 8 Deformed Shape of
Ring Stiffened Model at 100 psig

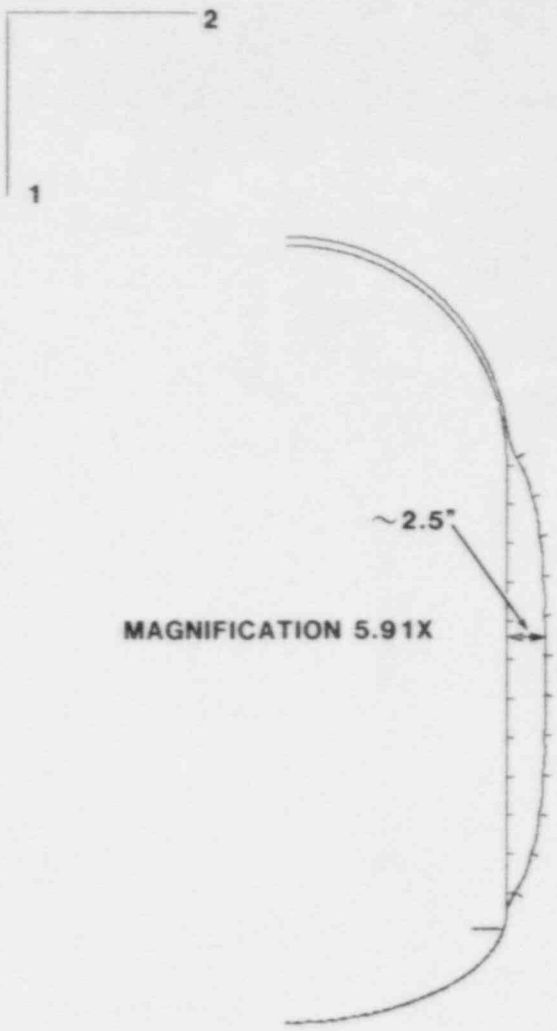

Figure 9 Deformed Shape of
Ring Stiffened Model at 200 psig

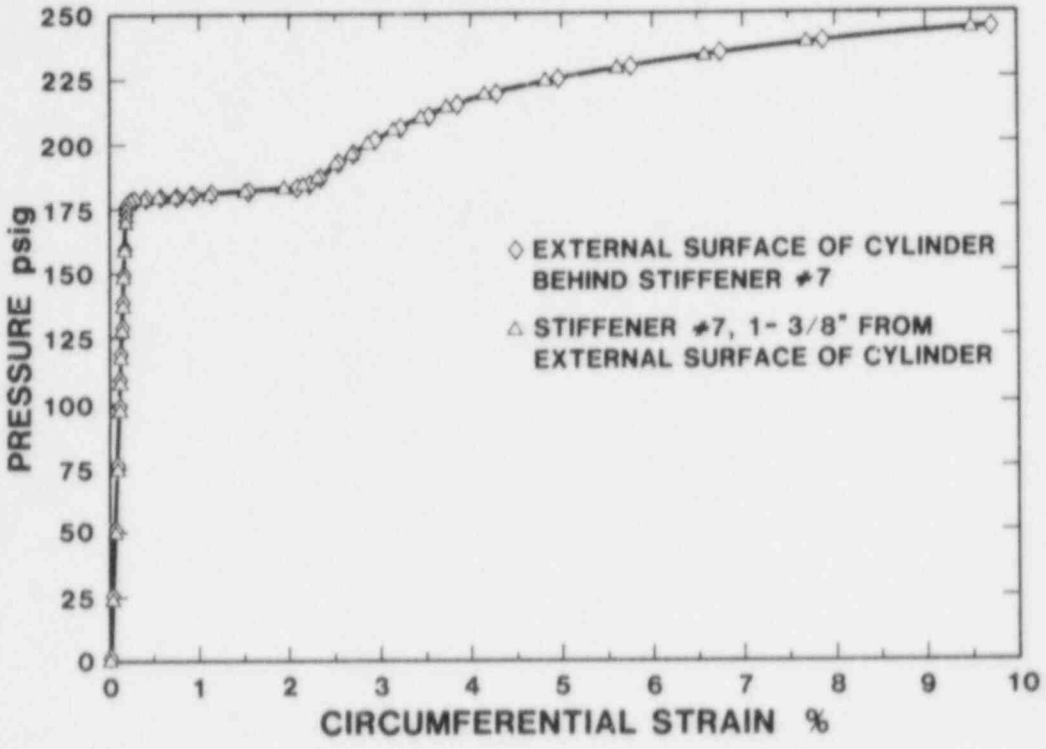

Figure 10 Circumferential Strain in Cylinder and Stiffener at the Same Elevation (Stiffener 7)

6.2 Equipment Hatch Covers

The equipment hatch covers and the tensioning rings were considered to be structurally uncoupled from the sleeve. This assumption implies that only normal loads are transmitted at the sealing surfaces, i.e., frictionless contact, and it permits deformation of the sleeve relative to the cover. Two other options for modeling the contact were not exercised: (1) friction could have been taken into account, which would have been difficult to quantify (coefficient of friction between the organic seal and steel would not have been well defined) and implement (friction/gap elements would have complicated the model), or (2) the sleeve and cover could have been treated as though they were rigidly connected, which would have prevented relative motion of the sealing surfaces. Uncoupling the sleeve and cover allowed for a tremendous simplification in the modeling requirements, while still retaining the important features of the deformation mechanics. The finite element mesh of the cover and tensioning ring is shown in Figure 11. The cover was modeled with 10 axisymmetric thin shell elements, and the tensioning ring was modeled with 18 eight node axisymmetric continuum elements, resulting in 176 degrees of freedom. The boundary conditions are also indicated in Figure 11.

The cover assembly in the scale model is much stiffer than those used in actual containments. The thickness of the cover had to be increased because of the method of attachment. As a

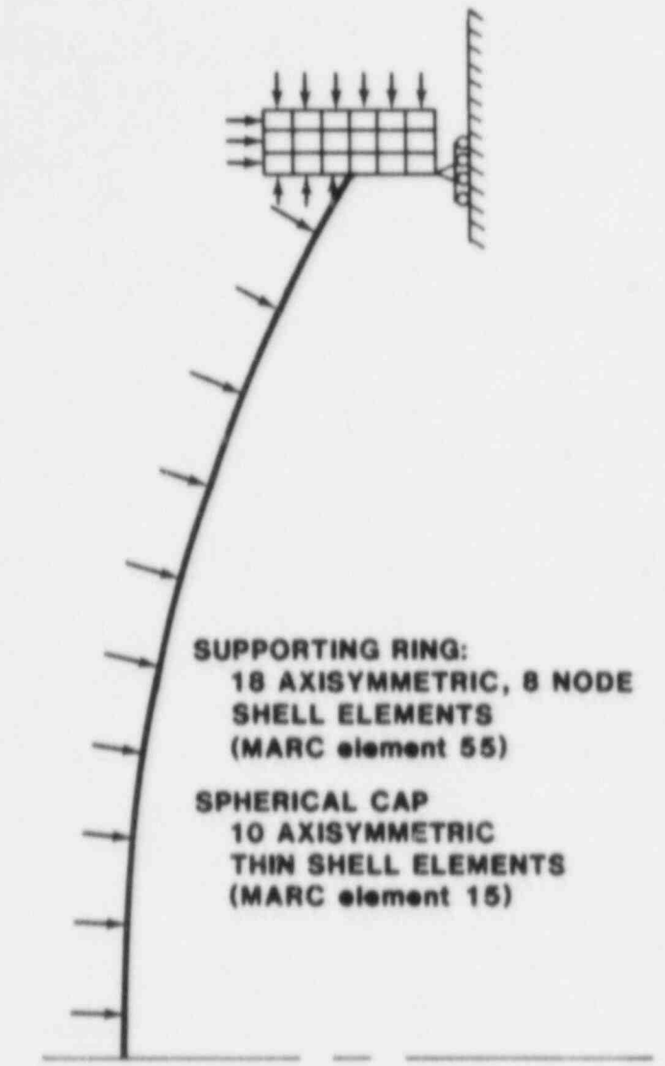

Figure 11 Finite Element Mesh for Equipment Hatch Cover

result, the response of the cover and tensioning ring was linear up to 360 psig, which is well above the predicted capacity of the scale model. First yield was associated with bending in the cover at its attachment to the tensioning ring; general yielding of the cover would have occurred at still higher pressure. Figure 12 shows that the tensioning ring moved radially outward only .00538 inches at 250 psig. Rotation of the tensioning ring was also negligible. The critical pressure for buckling of the cover was estimated at approximately 3000 psig.

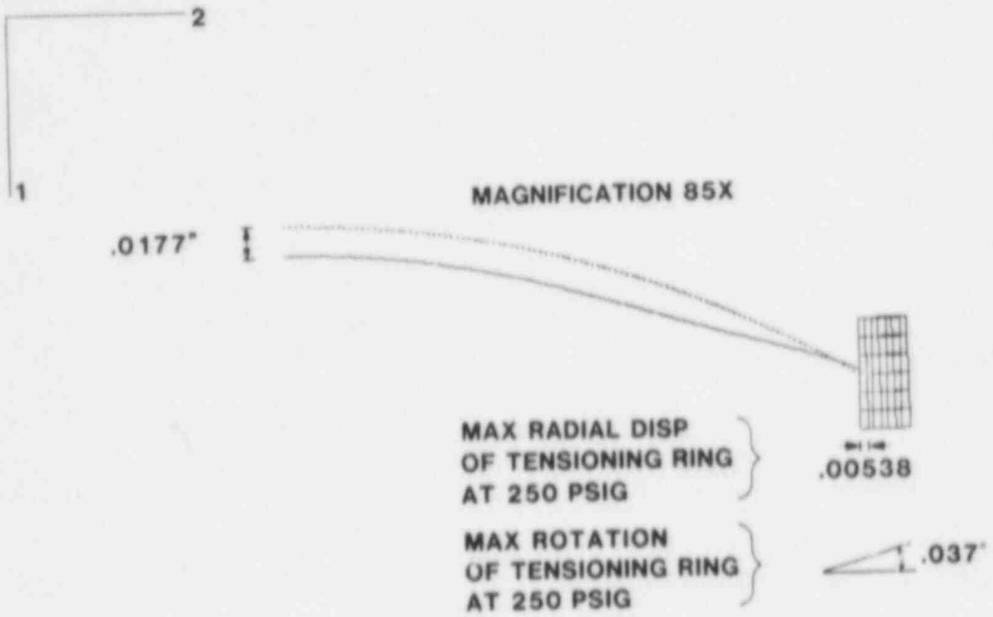

Figure 12 Deformed Shape of Equipment Hatch Cover at 250 psig

7. THREE-DIMENSIONAL MODELS

Three-dimensional analysis is necessary to correctly represent the mechanics of the interaction between a penetration and the cylinder. For example, the ovalization of the equipment hatch sleeve cannot be predicted with an axisymmetric model. The constrained pipe, the equipment hatches, and the upper personnel lock (PL2) were each analyzed separately. In addition, a model with a constrained pipe and an equipment hatch was analyzed in order to evaluate possible interaction between penetrations. MARC element 72, which is an 8 node, bilinear constrained thin shell element [13], was used exclusively in the three-dimensional models. This element has finite strain and large displacement capabilities.

7.1 Constrained Pipe

The effect of the constrained pipe on the cylinder is not localized, and therefore a 90° segment of the cylinder, which provides geometric symmetry, was modeled. Figure 13 shows the mesh used to predict the response of the cylinder and the

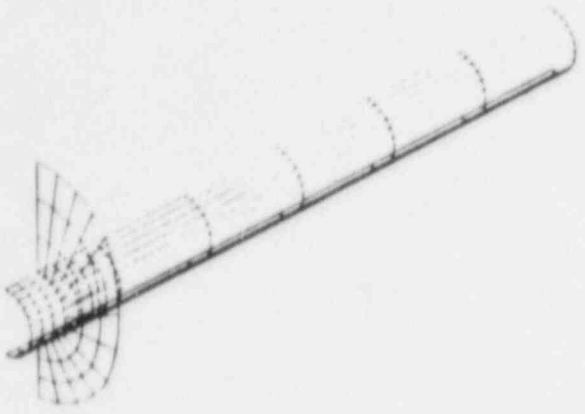

DETAIL OF CONSTRAINED PIPE AND REINFORCEMENT

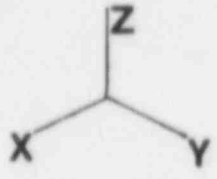

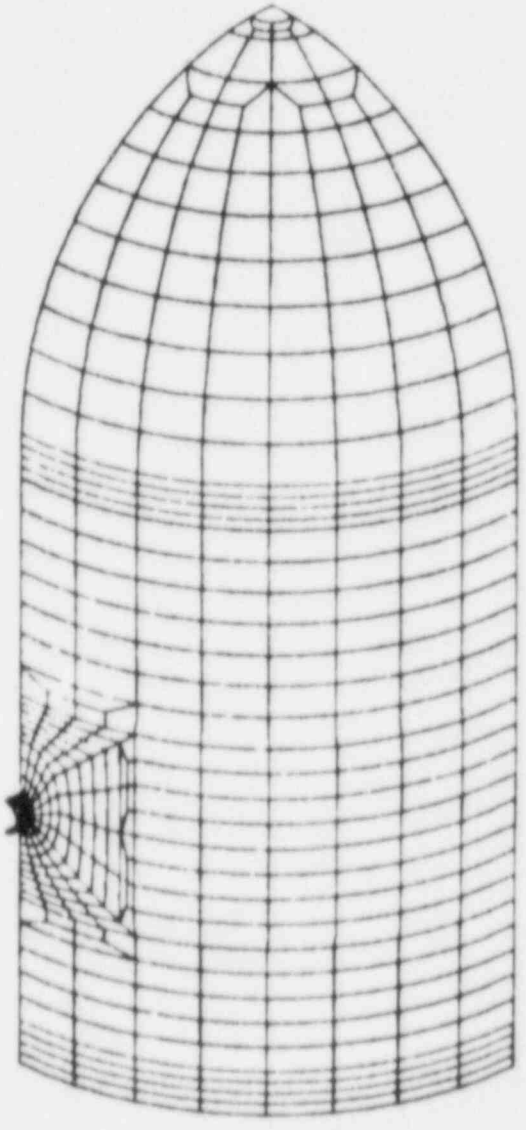

Figure 13 Finite Element Mesh for Constrained Pipe Model (CPM)

constrained pipe. The model includes 563 elements with 3074 active degrees of freedom. Ring stiffeners were modeled implicitly by increasing the thickness of the cylinder from 0.197 inch to 0.229 inch. This is an increase of 16%, which is the ratio of the volume of the stiffener material to the volume of the cylinder material. The pipe cover was accounted for by fixing the y displacements and forcing all z displacements to be equal for the nodes at end of the pipe outside of the cylinder. Pressure was applied to the convex surface of the part of the pipe inside the cylinder, as well as to the internal surfaces of the cylinder and dome. The constraint of the ellipsoidal base on the cylinder was modeled by fixing all translations at the lower springline. The behavior of the cylinder and of the constrained pipe is not affected by the boundary condition used for rotation except in the immediate vicinity of the lower springline, because

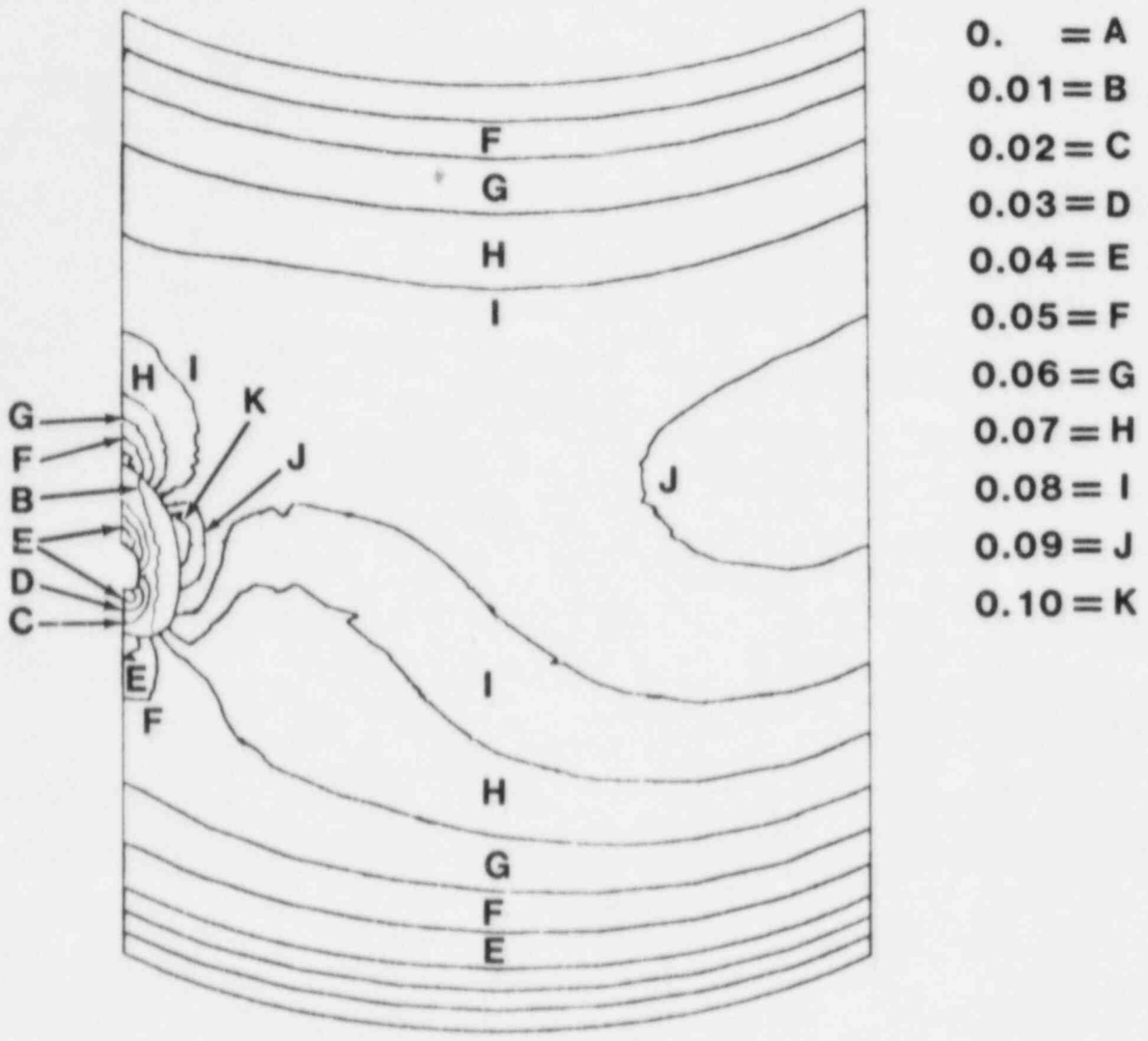

Figure 16 Midsurface Equivalent Plastic Strain Contours at 250 psig (CPM)

First yield occurred at 132 psig on the concave surface of the constrained pipe near its intersection with the reinforcement at 12 o'clock. At 250 psig, the maximum strain in the sleeve was only slightly less than the maximum strain in the cylinder. The large strains in the sleeve were very localized bending strains. Bending strains in penetration sleeves are discussed in section 6.2 in some detail. The constrained pipe, away from its intersection with the cylinder, remained elastic through 250 psig.

There is little or no loss in the capacity of the scale model associated with the constrained pipe.

7.2 Equipment Hatch Sleeve

The finite element mesh used to model the interaction of the equipment hatch sleeve and the cylinder is shown in Figure 17. The model includes 729 elements with 3894 active degrees of freedom. The ring stiffeners adjacent to the equipment hatch were modeled explicitly because preliminary analyses had demonstrated that the response of the equipment hatch sleeve was affected by the manner in which the stiffeners were modeled. The ring stiffeners near the upper and lower springline were modeled implicitly to reduce the size of the model. The purpose in explicitly modeling the stiffeners near the equipment hatch was to better predict their effect on the cylinder and equipment hatch sleeve. Some simplifications were made in modeling the geometry of the formed stiffener around the equipment hatch, and the mesh refinement used to model the stiffeners was probably not

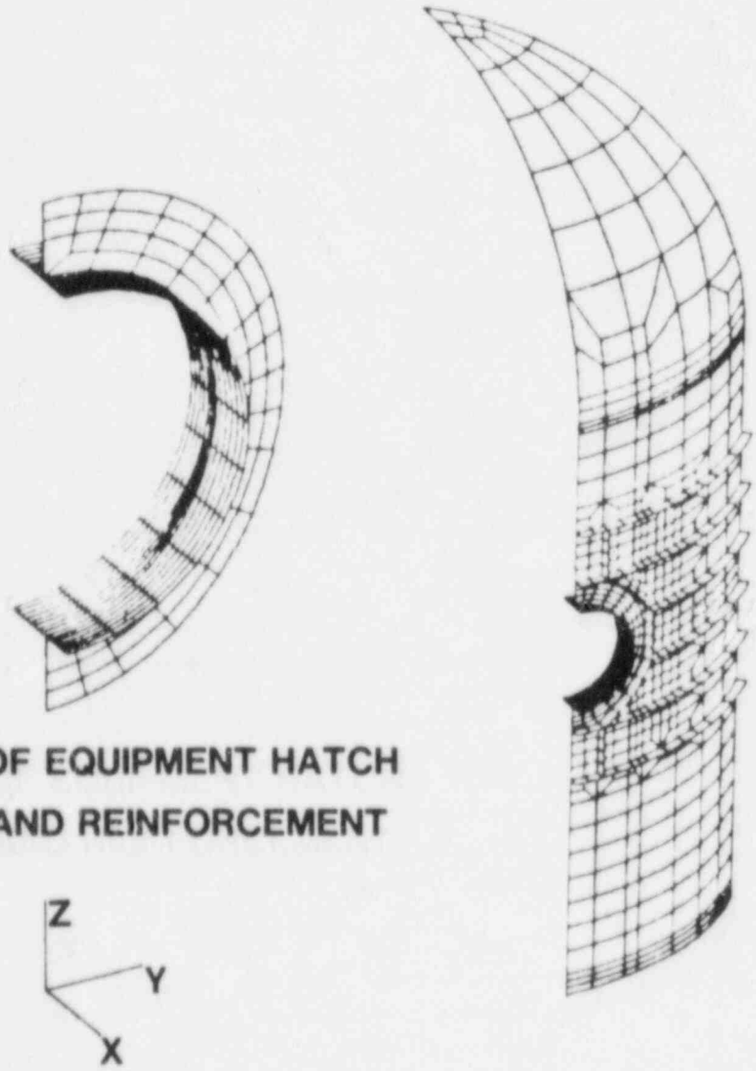

Figure 17 Finite Element Mesh for Equipment Hatch Model (EHM)

it only affects the bending response, which is highly localized. The rotation of the cylinder at the lower springline was not constrained since it was not necessary to accurately model the bending at this point. (The cylinder's response at the lower springline was predicted with an axisymetric model, see Section 6.1.) Because of geometric symmetry, no tangential displacement or rotation of the boundaries at 0° and 90° was allowed. The radial displacement and rotation of the dome apex and the constrained pipe at the center of the cylinder were fixed.

The constrained pipe did not affect general membrane yielding of the cylinder; the membrane yield pressure for the constrained pipe model was 180 psig, exactly the same as for the ring stiffened axisymmetric model. The deformed shape at 250 psig is shown in Figure 14 superposed on the outline of the undeformed shape. The cylinder was essentially fixed at its

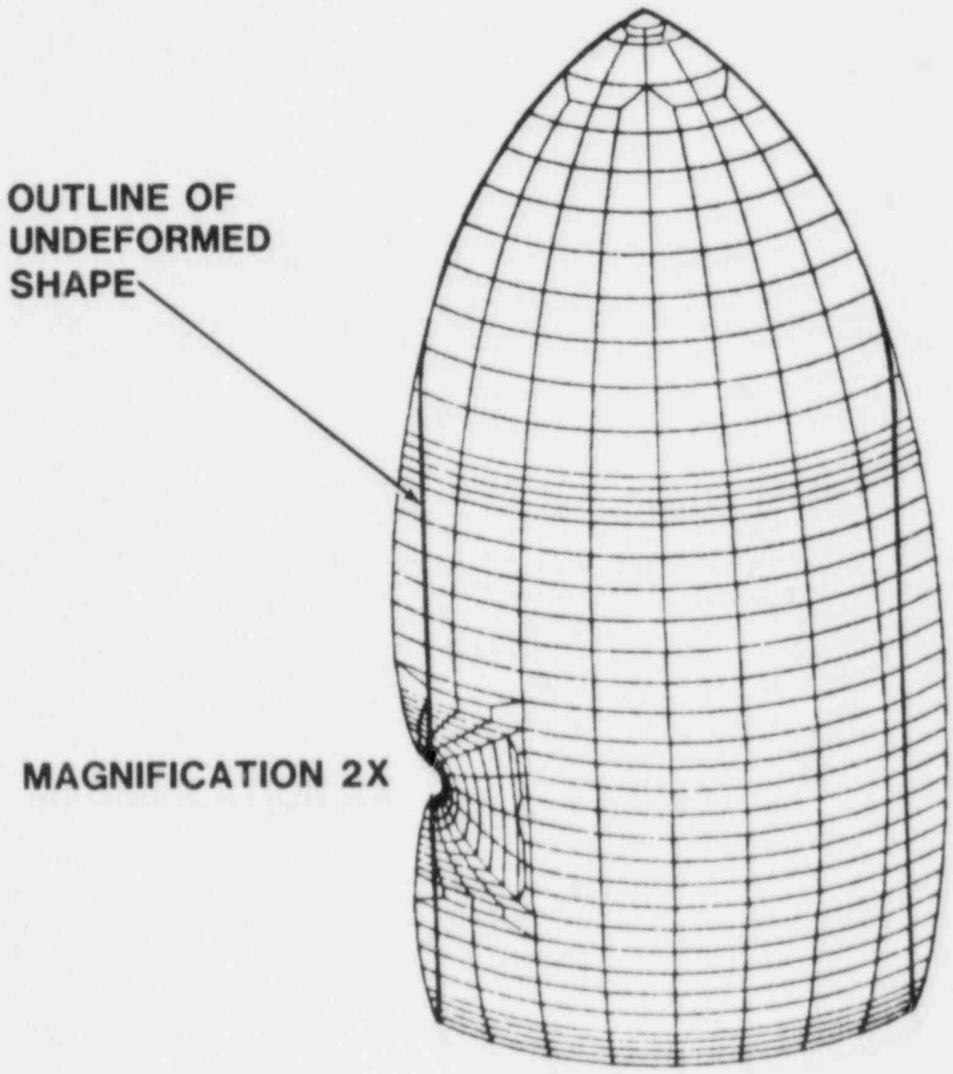

Figure 14 Deformed Shape at 250 psig (CPM)

intersection with the constrained pipe. The pipe restricted bulging of the cylinder even at points well away from the penetration, Figure 15, with the effect being more pronounced at higher pressures.

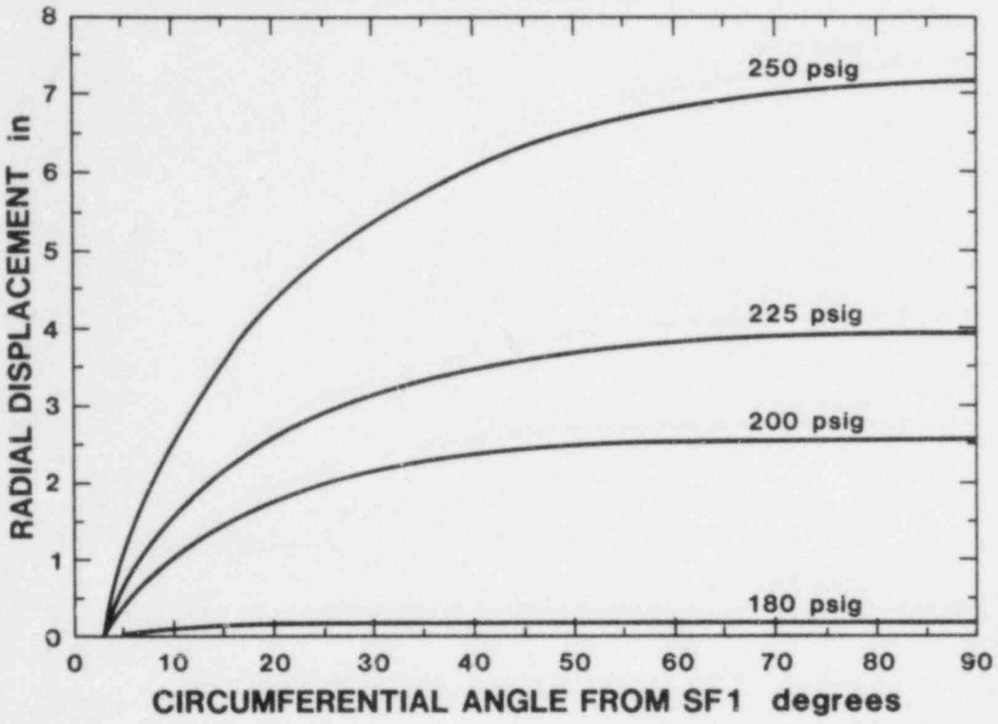

Figure 15 Circumferential Variation of Radial Displacement at the Elevation of the Constrained Pipe

Midsurface plastic strain contours at 250 psig are plotted for the cylinder and reinforcement in Figure 16. The strains were less at most points on the cylinder than those predicted with the ring stiffened model at the same elevation. The maximum strain in the constrained pipe model was associated with the strain concentration in the cylinder adjacent to the reinforcement. Similar strain concentrations were predicted around the reinforcements for the other penetrations that were analyzed. These strain concentrations are related to the difference in the membrane response of the cylinder and reinforcement. Because the reinforcement is thicker than the cylinder, the radial expansion associated with its membrane response is less than for the cylinder. This causes a mismatch in the tangential displacement of the cylinder and reinforcement, which is compensated for by additional circumferential stretching (straining) of the cylinder. The strain is accumulated in the cylinder because the reinforcement is much stiffer as result of its greater thickness.

sufficient to allow an accurate prediction of the strains in the stiffeners themselves. As discussed in section 5.2, the sleeve and cover were treated as structurally uncoupled. A line load oriented parallel to the sleeve axis was applied to the inside end of the sleeve to account for the pressure acting on the cover. Pressure was applied to the convex surface of the sleeve that is inside the cylinder, and also to the internal surface of the cylinder and dome. Symmetry boundary conditions (no tangential displacement or rotation about the edge) were applied to the boundaries at 0° and 48°. The boundary condition at 0° was based on geometric symmetry. The circumferential extent of the model was selected so that the state of stress and displacement along the other boundary were not affected by the penetration, i.e., the response at the boundary was axisymmetric. Comparisons of preliminary results for a ring stiffened model with those for an equipment hatch model demonstrated that a 48° segment was large enough to justify the symmetry condition. Translation of the cylinder was fixed at the lower springline, and rotation was permitted. The apex of the dome was restricted to motion in the axial direction only.

Figure 18 shows the deformed shape of the equipment hatch sleeve at 225 psig. The sleeve deformed into a distinct oval shape, except at its intersection with the reinforcement, which restricted the ovalization of the sleeve at 6 and 12 o'clock. Because the ends of the sleeve were assumed to be unrestrained, the sleeve could deform into an oval shape (inextensional mode), which is a relatively flexible mode of deformation. On the other hand, the response of the cylinder and reinforcement was charac-

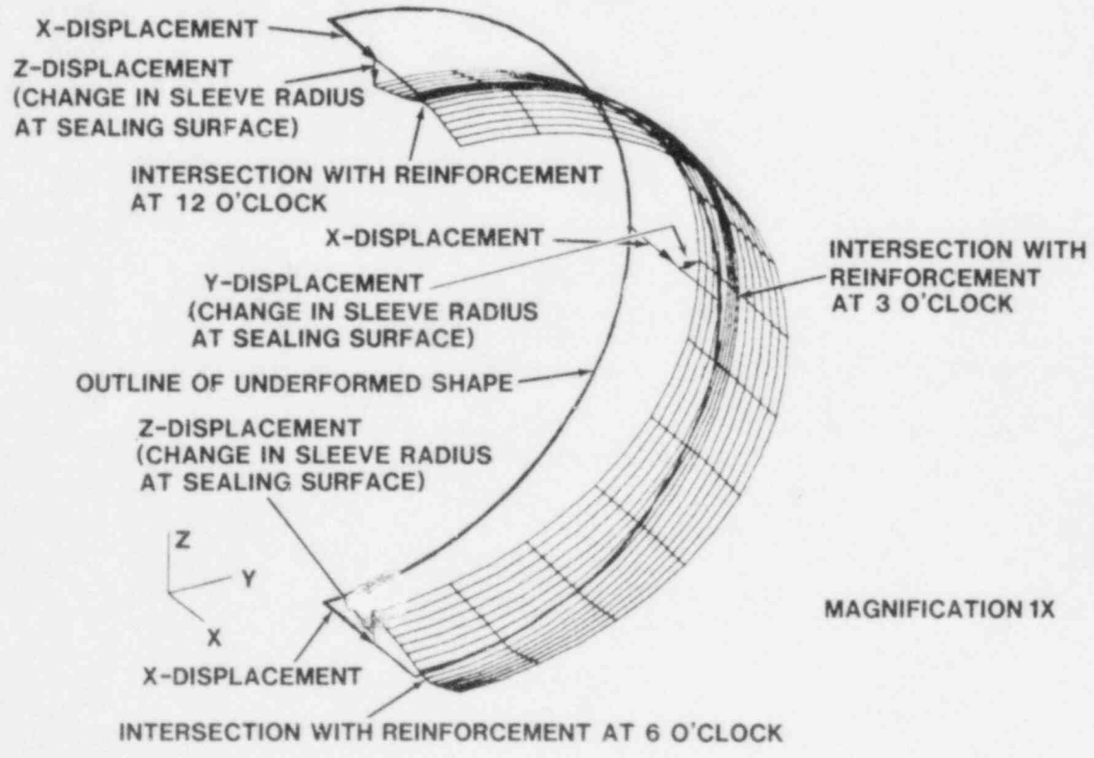

Figure 18 Deformed Shape of Equipment Hatch Sleeve at 225 psig

terized by membrane action, which is a much stiffer mode than the inextensional mode. Therefore, the sleeve was forced to conform to the deformed shape of the cylinder and reinforcement. As indicated in Figure 19, as the cylinder and reinforcement expand, the sleeve diameter from 3 to 9 o'clock must increase. This stretching of the horizontal diameter had an effect similar to pinch loads, causing the sleeve to ovalize. However, the

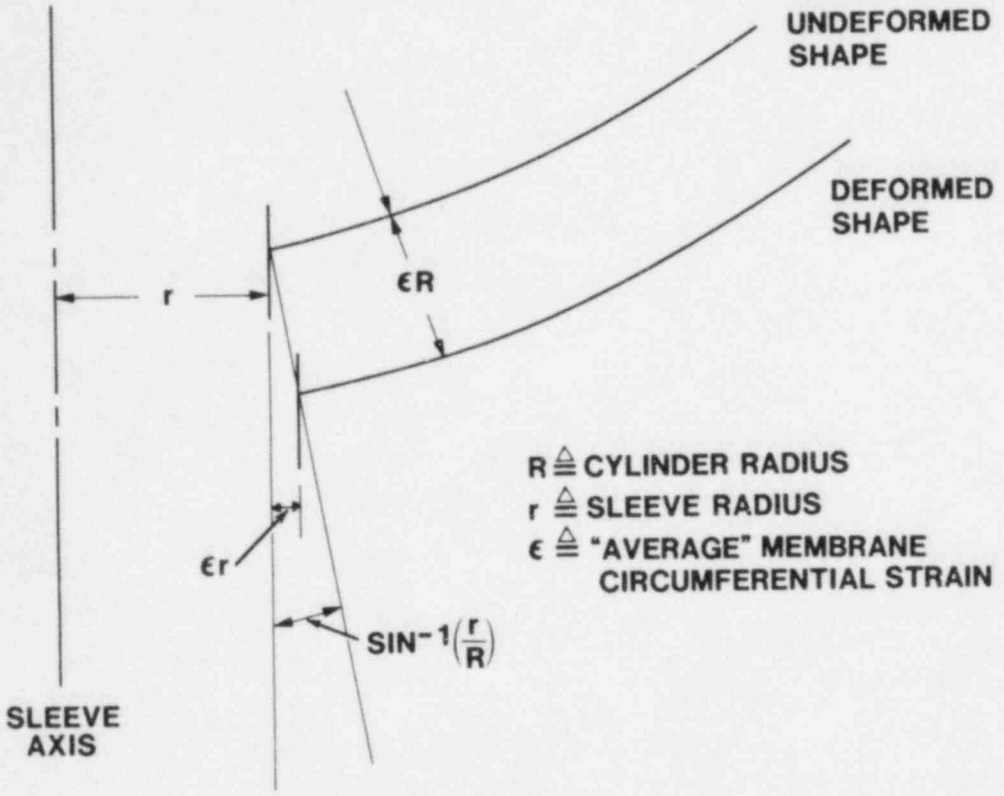

Figure 19 Sleeve - Cylinder Interaction

cylinder and reinforcement did not stretch in the meridional direction, and consequently the vertical sleeve diameter was not allowed to change at the intersection with the cylinder. This restriction causes high bending strains in the sleeve at the 6 and 12 o'clock positions near the intersection with the reinforcement. At the end of the sleeve inside the cylinder (the sealing surface), large changes in the vertical and horizontal diameter occurred as a result of the ovalization. As discussed in Section 5.2, the equipment hatch cover tensioning rings were effectively rigid. Therefore, leakage from the equipment hatch 'O' ring seals was expected by 210 psig, when the decrease in the vertical diameter of the end of the sleeve exceeded twice the sleeve thickness, Figure 20. This deformation causes a complete mismatch between the sleeve and the tensioning ring.

First yield occurred in the sleeve near its intersection with the reinforcement at 51.5 psig. Figure 21 shows the equivalent plastic strain contours at 225 psig in the equipment

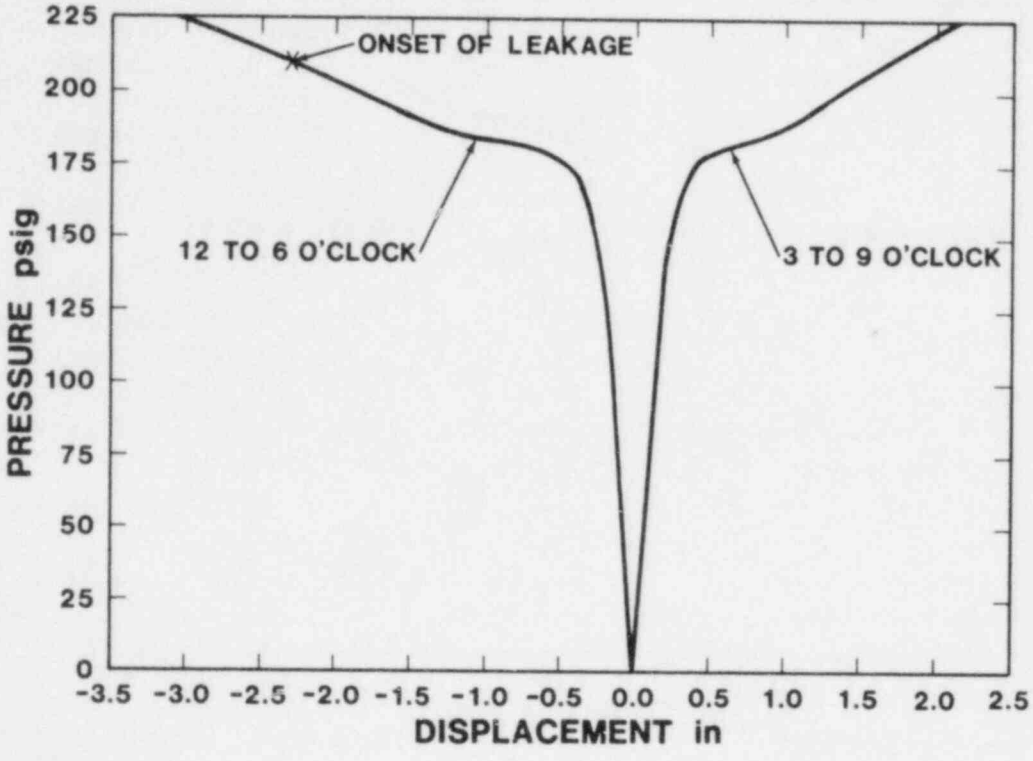

Figure 20 Change in EH Sleeve Diameter Adjacent to Seal

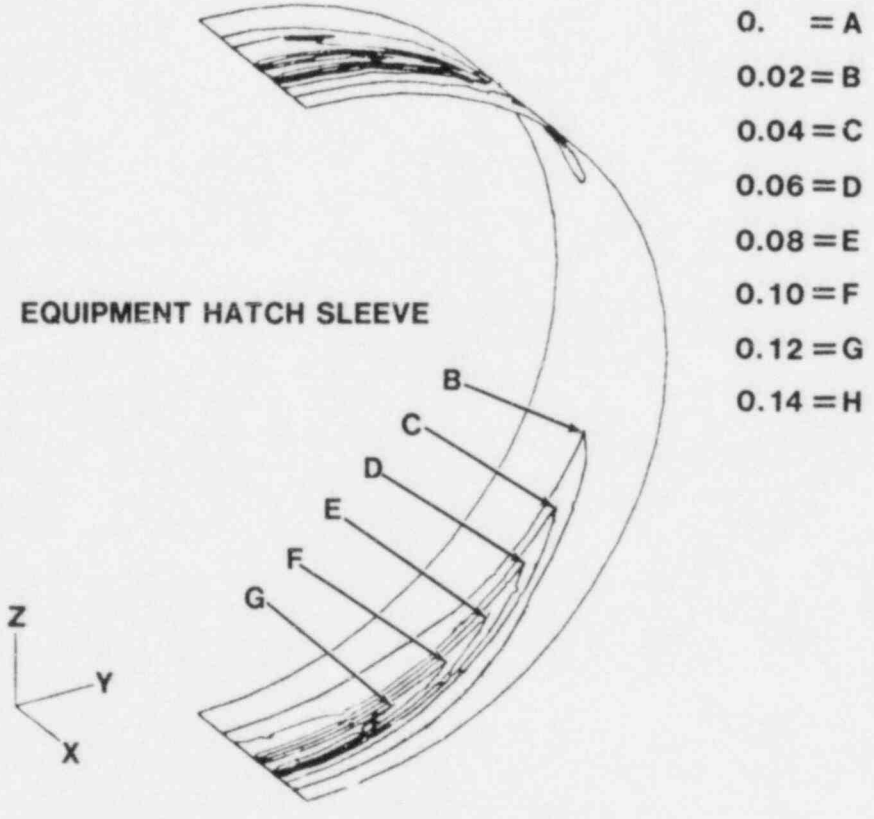

Figure 21 Concave Surface Equivalent Plastic Strain Contours at 225 psig (EHM)

hatch sleeve. The major component of strain was meridional strain due to bending. Note that the large strains are localized to the area of the sleeve near its intersection with the reinforcement at 6 and 12 o'clock. Although yielding occurred at a relatively low pressure level, the strains in the sleeve did not increase substantially until after membrane yielding of the cylinder occurred. This behavior was typical of all three penetration sleeves that were analyzed, as shown in Figure 22. The maximum strain in a penetration sleeve at a given pressure level is roughly proportional to the thickness to radius ratio of the sleeve at its intersection with the reinforcement [10]. Other factors that influenced the bending strain in penetration sleeves were the details of the sleeve materials' stress-strain curves, the width and thickness of reinforcement, the boundary conditions on the ends of the sleeve, and the stiffener details around the penetration.

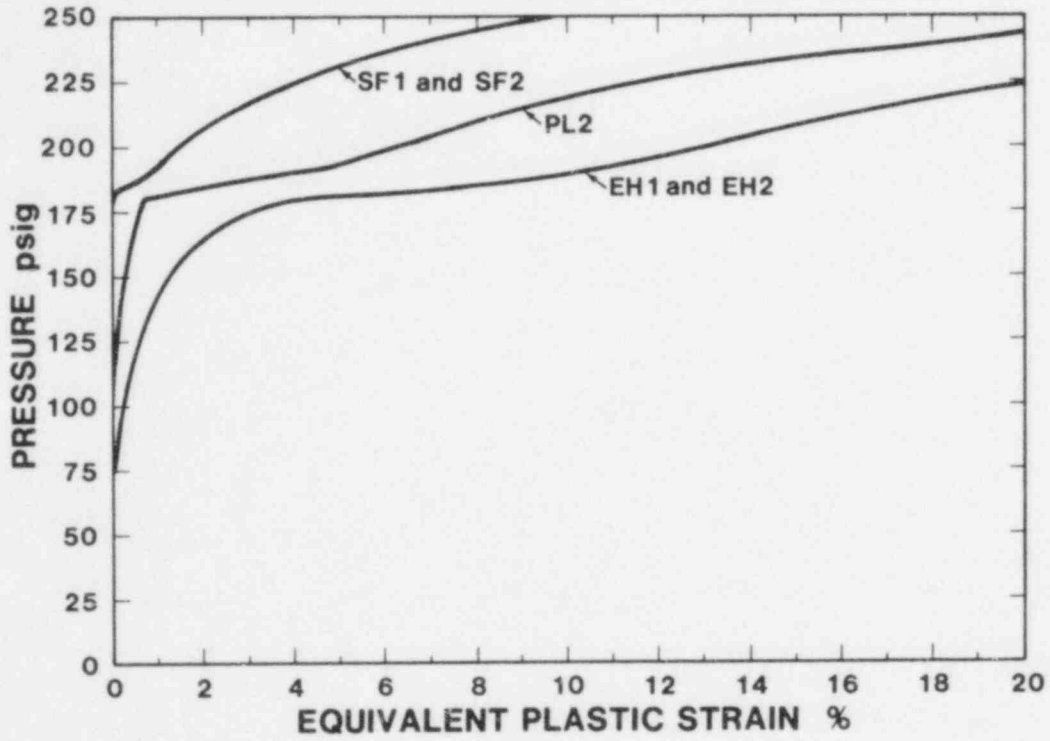

Figure 22 Strain on Concave Surface of Penetration Sleeves at 12 O'clock at their Intersection with the Reinforcement

The deformed shape superposed on an outline of the undeformed shape, and the strain contours for the reinforcement and the cylinder at 225 psig are shown in Figures 23 and 24, respectively. The perturbation caused by the equipment hatch penetration was localized. Strain concentrations arose in the cylinder at the elevation of the center of the equipment hatch adjacent to the reinforcement, and in the reinforcement immediately above and below the intersection with the sleeve.

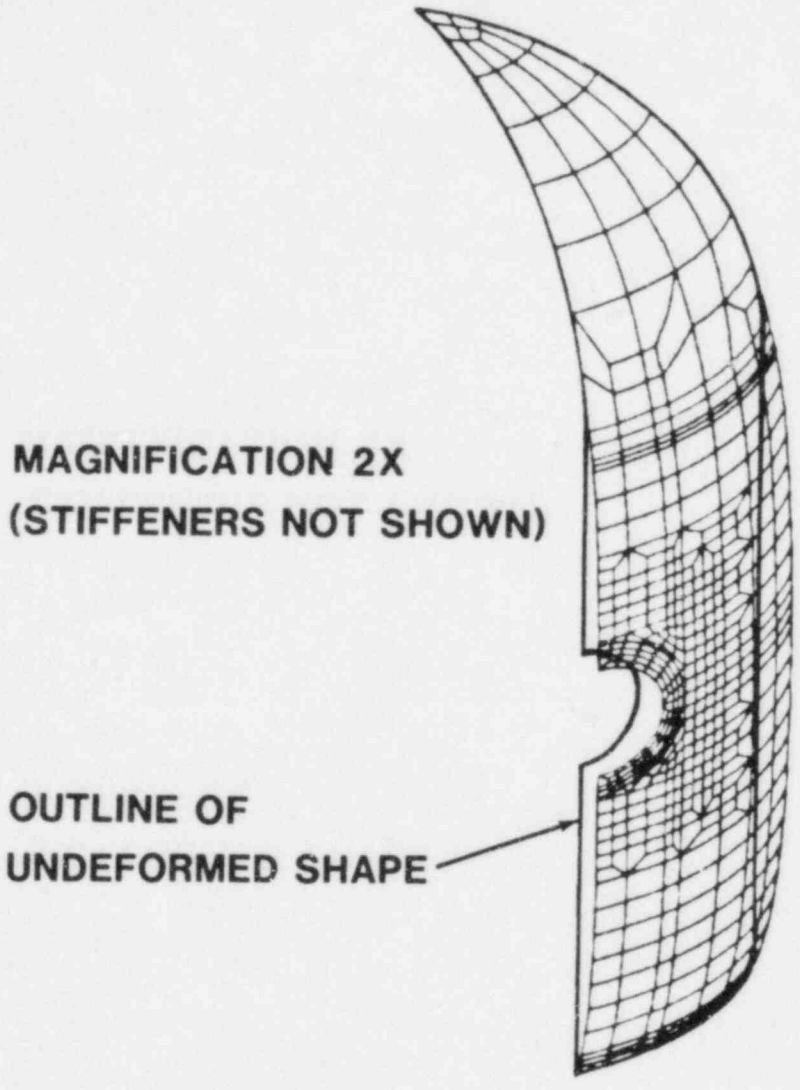

Figure 23 Deformed Shape at 225 psig (EHM)

hatch sleeve. The major component of strain was meridional strain due to bending. Note that the large strains are localized to the area of the sleeve near its intersection with the reinforcement at 6 and 12 o'clock. Although yielding occurred at a relatively low pressure level, the strains in the sleeve did not increase substantially until after membrane yielding of the cylinder occurred. This behavior was typical of all three penetration sleeves that were analyzed, as shown in Figure 22. The maximum strain in a penetration sleeve at a given pressure level is roughly proportional to the thickness to radius ratio of the sleeve at its intersection with the reinforcement [10]. Other factors that influenced the bending strain in penetration sleeves were the details of the sleeve materials' stress-strain curves, the width and thickness of reinforcement, the boundary conditions on the ends of the sleeve, and the stiffener details around the penetration.

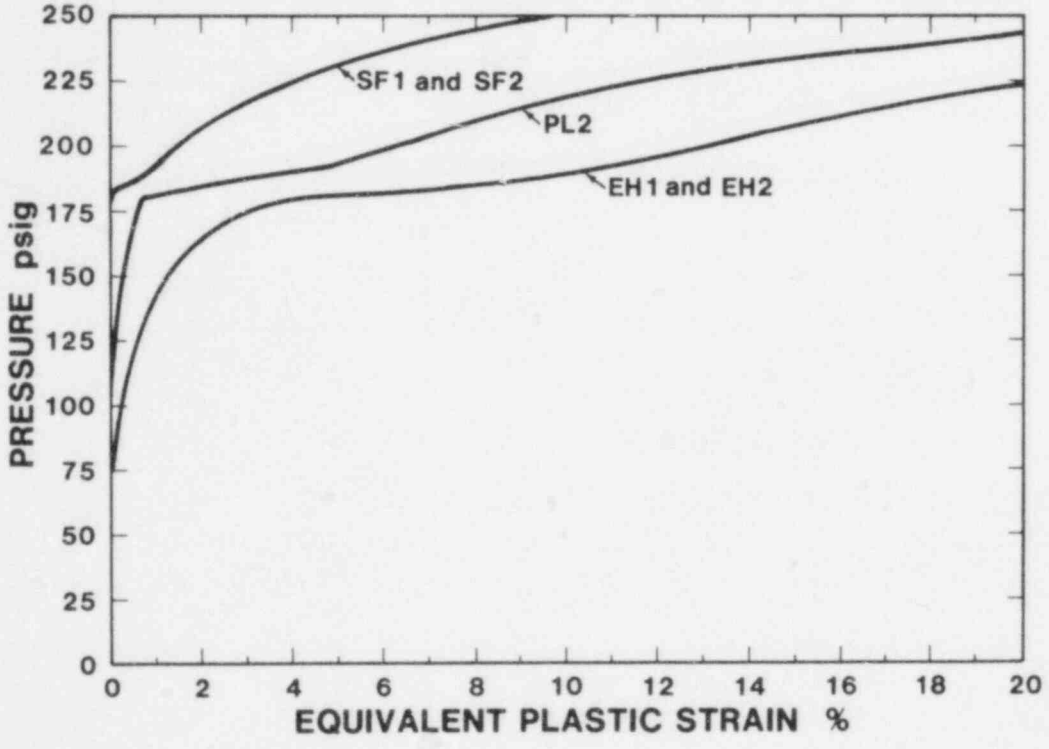

Figure 22 Strain on Concave Surface of Penetration Sleeves at 12 O'clock at their Intersection with the Reinforcement

The deformed shape superposed on an outline of the undeformed shape, and the strain contours for the reinforcement and the cylinder at 225 psig are shown in Figures 23 and 24, respectively. The perturbation caused by the equipment hatch penetration was localized. Strain concentrations arose in the cylinder at the elevation of the center of the equipment hatch adjacent to the reinforcement, and in the reinforcement immediately above and below the intersection with the sleeve.

The midsurface strain in the reinforcement and cylinder at the elevation of the center of the penetration is plotted in Figure 25 for several different pressure levels. The strain concentration factor is the maximum strain divided by the strain at 48°.

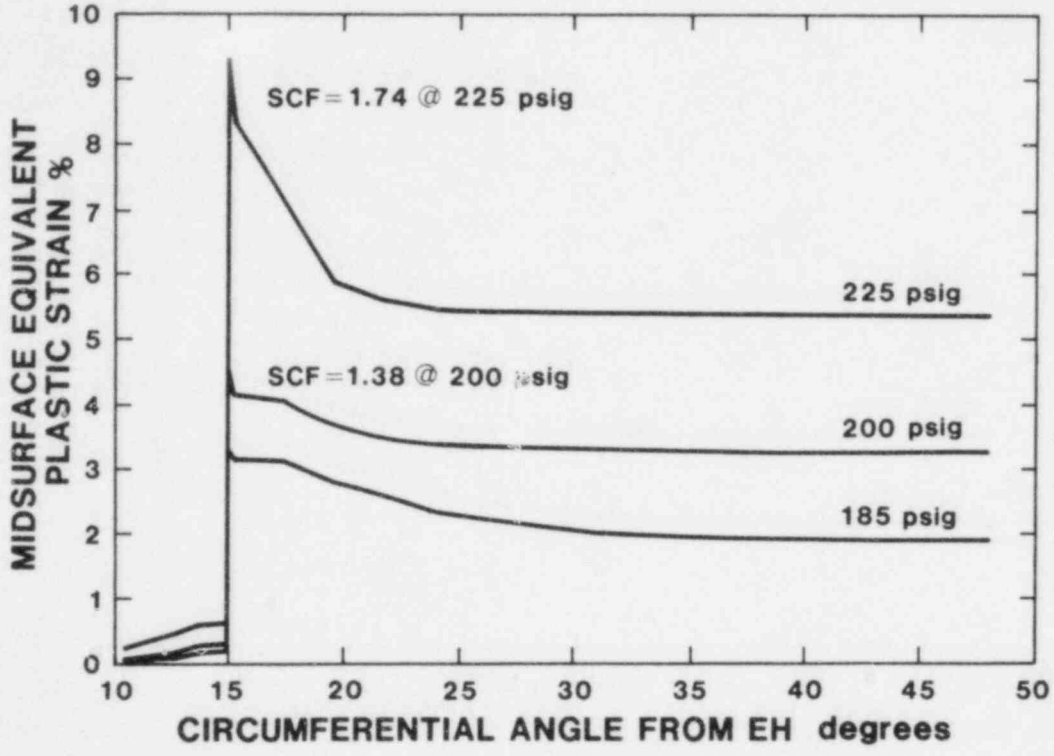

Figure 25 Circumferential Variation in the Strain at the Elevation of an Equipment Hatch

7.3 Personnel Lock at Midheight

The finite element mesh used to represent the cylinder with the upper personnel lock (PL2) is shown in Figure 26. The model includes 381 elements with 2119 active degrees of freedom. Ring stiffeners were implicitly modeled. The nodes on each end of the sleeve were required to displace the same amount in the y and z directions, which simulated the effect of the covers on the sleeve. The pressure on the inside cover was accounted for by applying nodal loads at the end of the sleeve. The convex surface of the sleeve inside the cylinder and the internal surfaces of the cylinder and dome were subject to pressure loads. Symmetry conditions were used on the boundaries at 0° and 36°, for the same reasons that they were used on the boundaries of the equipment hatch model (see Section 6.2). The circumferential extent of the mesh is less because PL2 is a much smaller penetration than either equipment hatch, and consequently the effect of PL2 does not propagate as far into the cylinder as that of the equipment hatches. The boundary conditions for the cylinder at the lower springline and the apex of the dome are the same as those used for the other three-dimensional models.

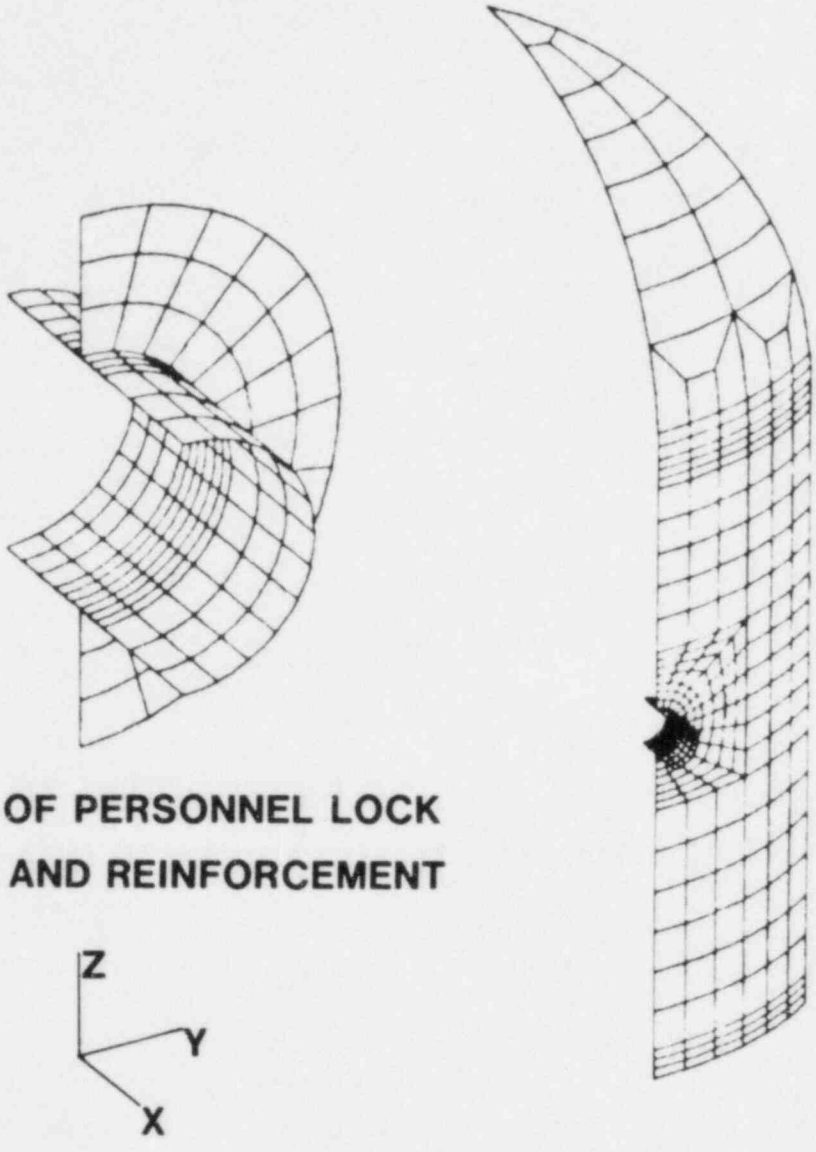

Figure 26 Finite Element Mesh for Personnel Lock Model (PLM)

First yield of the model occurred at 71.6 psig on the convex surface of the sleeve near its intersection with the reinforcement. As discussed in Section 6.2, the strains at this point are associated with localized bending. The magnitude of the maximum bending strain depended strongly on the radius to thickness ratio of the sleeve.

Strain contours in the reinforcement and cylinder at 250 psig are shown in Figure 27. Membrane yielding occurred at approximately 180 psig, just like the other models. The strain concentration factor (scf) can be determined from Figure 28. At 200 psig the scf was 1.54; by 250 psig the scf had increased to 1.74.

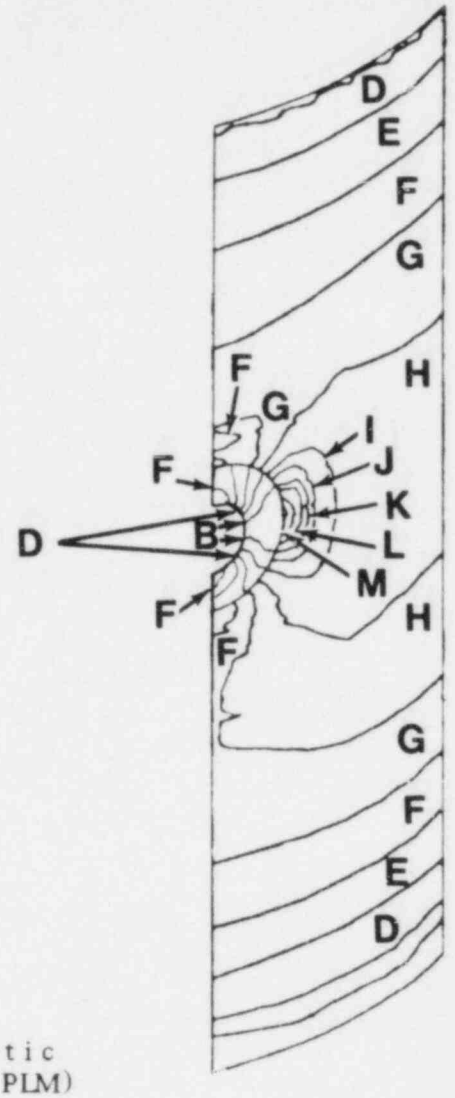

Figure 27 Midsurface Equivalent Plastic Strain Contours at 250 psig (PLM)

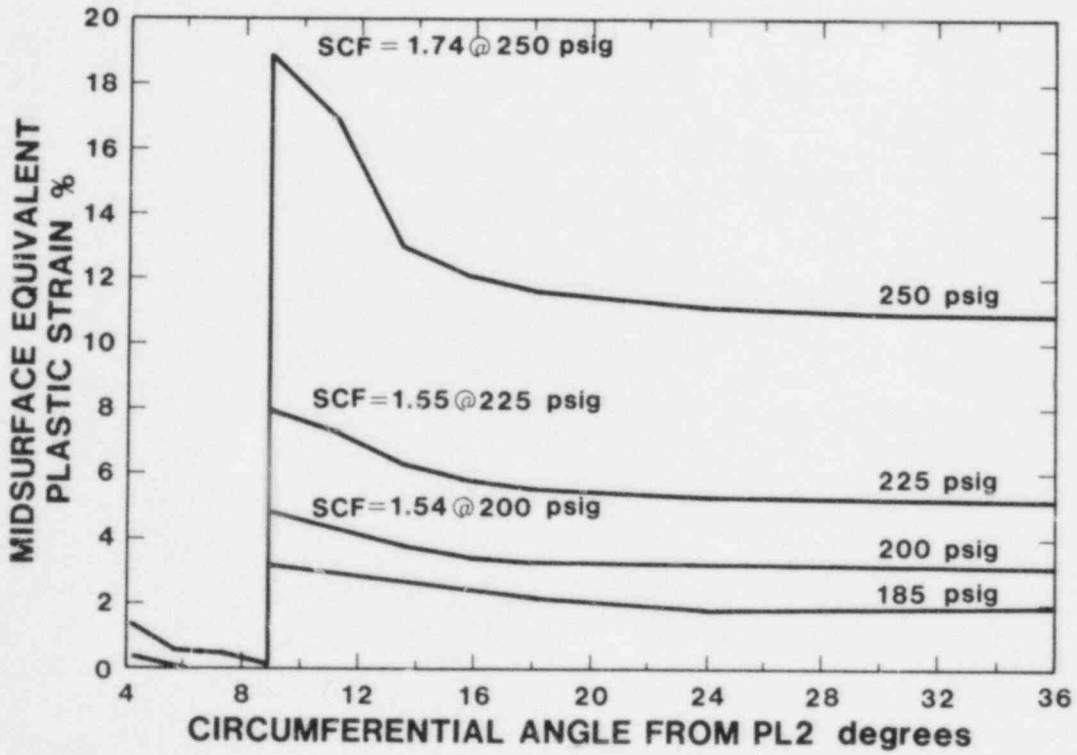

Figure 28 Circumferential Variation in the Strain at the Elevation of the Personnel Lock Near Midheight (PL2)

7.4 Penetration Interactions

Because the effect of the constrained pipe on the cylinder was not localized as it was for other penetrations, a model including the constrained pipe and an equipment hatch was analyzed to investigate to what degree they would interact. The finite element mesh is shown in Figure 29. The model consisted of 1017 elements with 5280 active degrees of freedom. The constrained pipe was not explicitly modeled; the radial and tangential displacement of the reinforcement along the edge where it intersected the pipe were fixed to simulate the fixity applied by the pipe. For reasons discussed in Section 6.2, three ring stiffeners below and three above the centerline of the equipment hatch were modeled explicitly, while the stiffeners near the upper and lower springlines were modeled implicitly. Nodal loads were applied to the inside end of the sleeve to account for the pressure acting on the equipment hatch cover, which was assumed to be structurally uncoupled from the sleeve (see Section 5.2). The convex surface of the equipment hatch sleeve inside the cylinder and the internal surfaces of the cylinder,

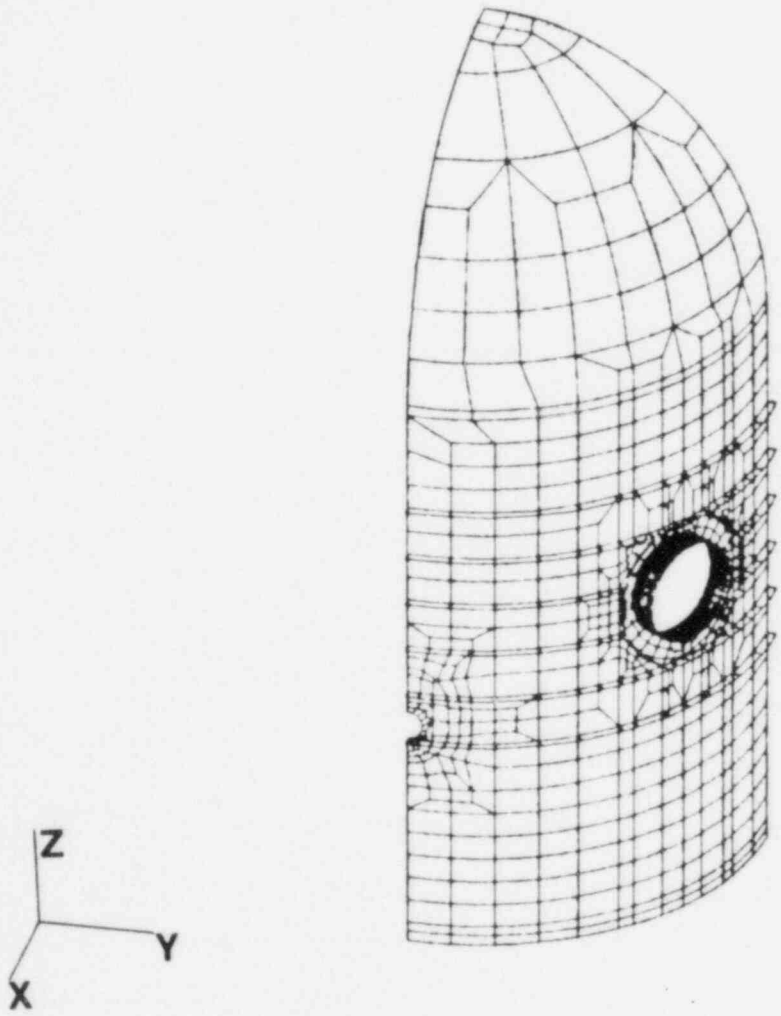

Figure 29 Mesh for Penetration Interaction Model (PIM)

reinforcements, and the dome were subject to pressure. Tangential displacement and rotation were fixed along the boundaries at 0° and 90°. The cylinder was not allowed to translate at the lower springline, although rotation was not constrained. The apex of the dome was restricted to motion in the axial direction only.

The analysis was terminated at 184 psig, which corresponded to a maximum membrane strain of approximately 1.5%, because there was no interaction between the equipment hatch and the constrained pipe and because the computing time associated with each increment were very large (on the order of 400 CRAY CPU seconds). Results from the equipment hatch model and the penetration interactions model are compared in Figures 30 thru 32 for several key areas. The dashed lines represent the results from the penetration interaction model in these figures and the two that follow. The similarity of the results for the two models shows that the response of the equipment hatch and the cylinder in its vicinity are not affected by the constrained pipe. Figures 33 and 34 demonstrate that the reverse is also true: The response of the cylinder near the constrained pipe is not affected by the equipment hatch, at least for small plastic strains. In retrospect, the absence of significant interaction up to 184 psig should not have been unexpected. Figure 15 shows that the effect of the constrained pipe does not propagate through the entire model until high pressures are reached and larger plastic strains are accumulated. At low pressures and small plastic strains, the equipment hatch was still in an essentially axisymmetric strain field. In view of Figure 25, interaction would be more likely to occur for pressures above 225 psig.

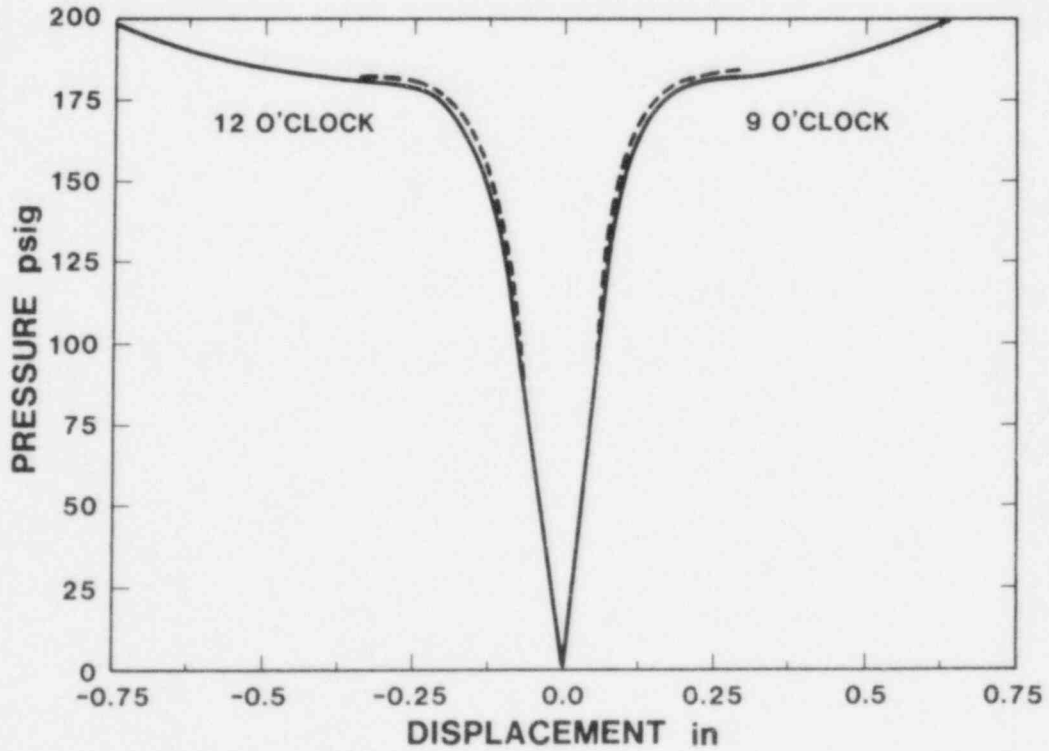

Figure 30 Change in EH Sleeve Radii Adjacent to Seal

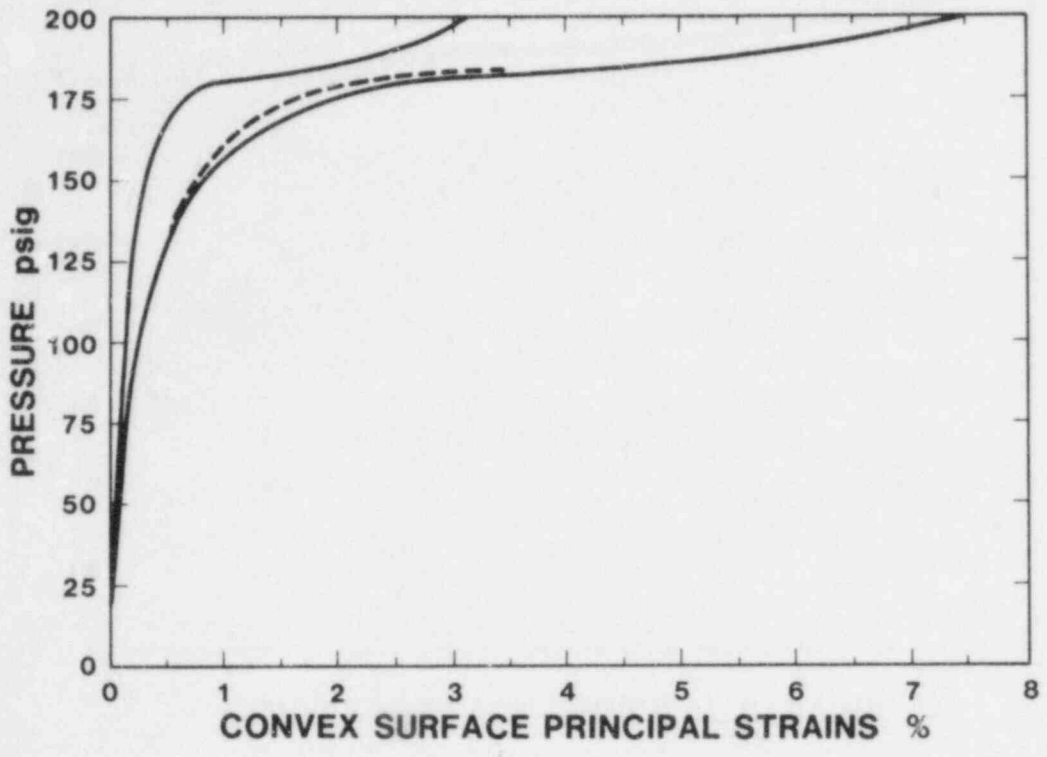

Figure 31 Comparison of EHM and PIM
Strains in EH Sleeve at Its Intersection with Reinforcement

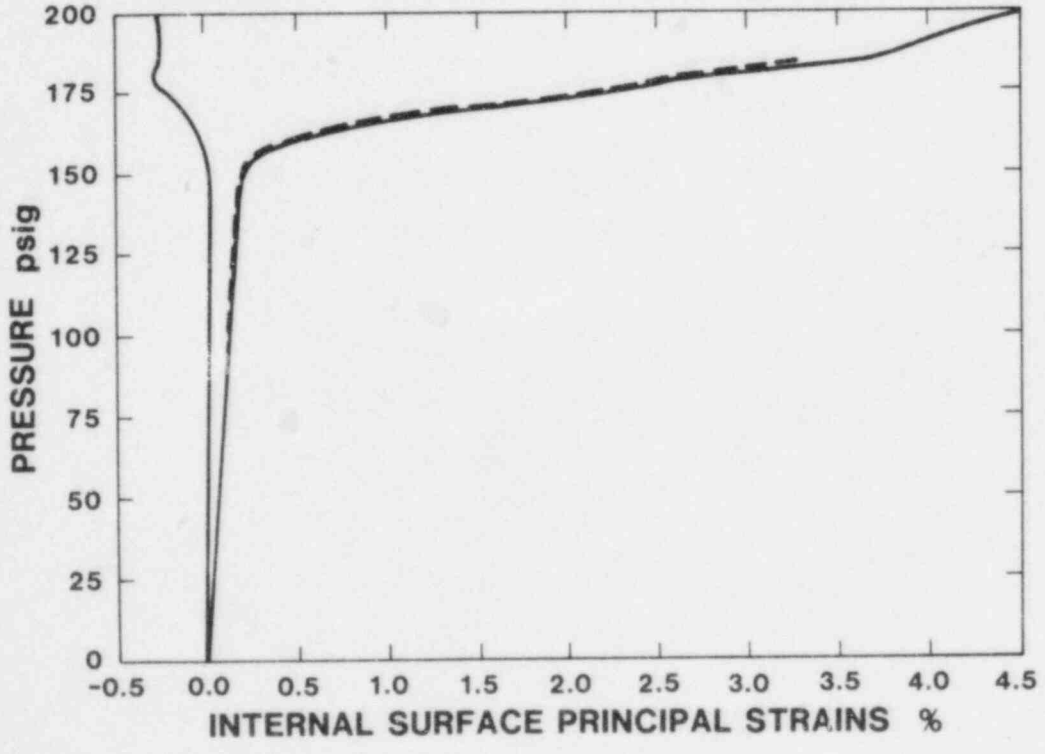

Figure 32 Comparison of EHM and PIM
Strain Concentration in CylinderAdajcent to EH Reinforcement

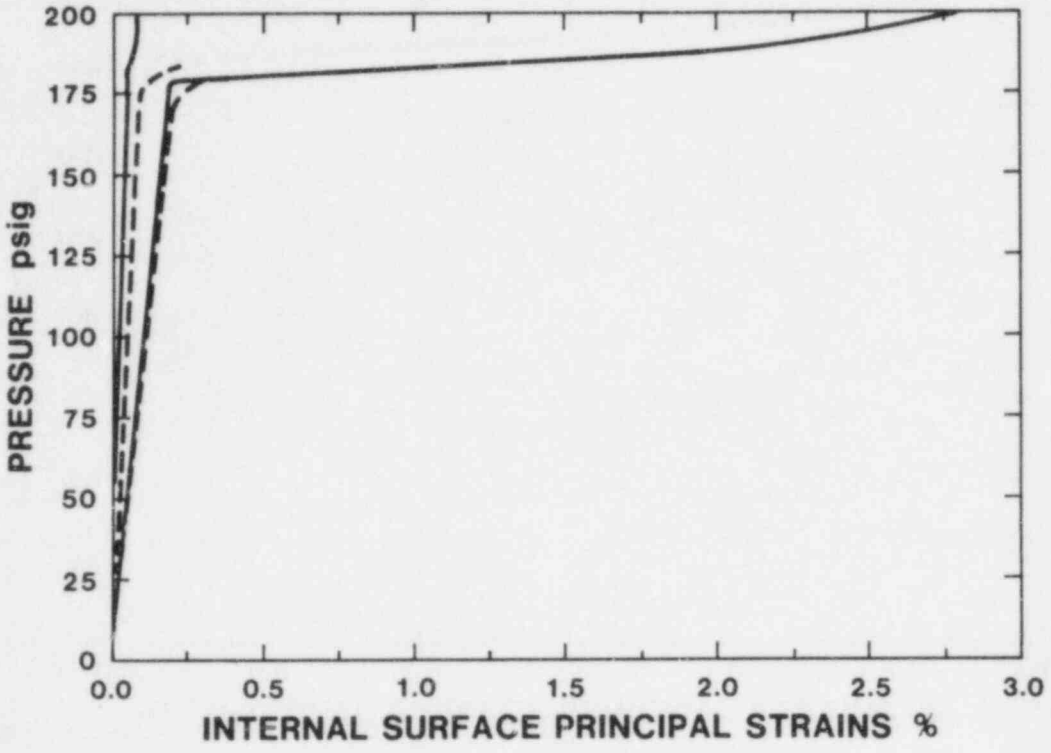

Figure 33 Comparison of CPM and PIM - Membrane Strain

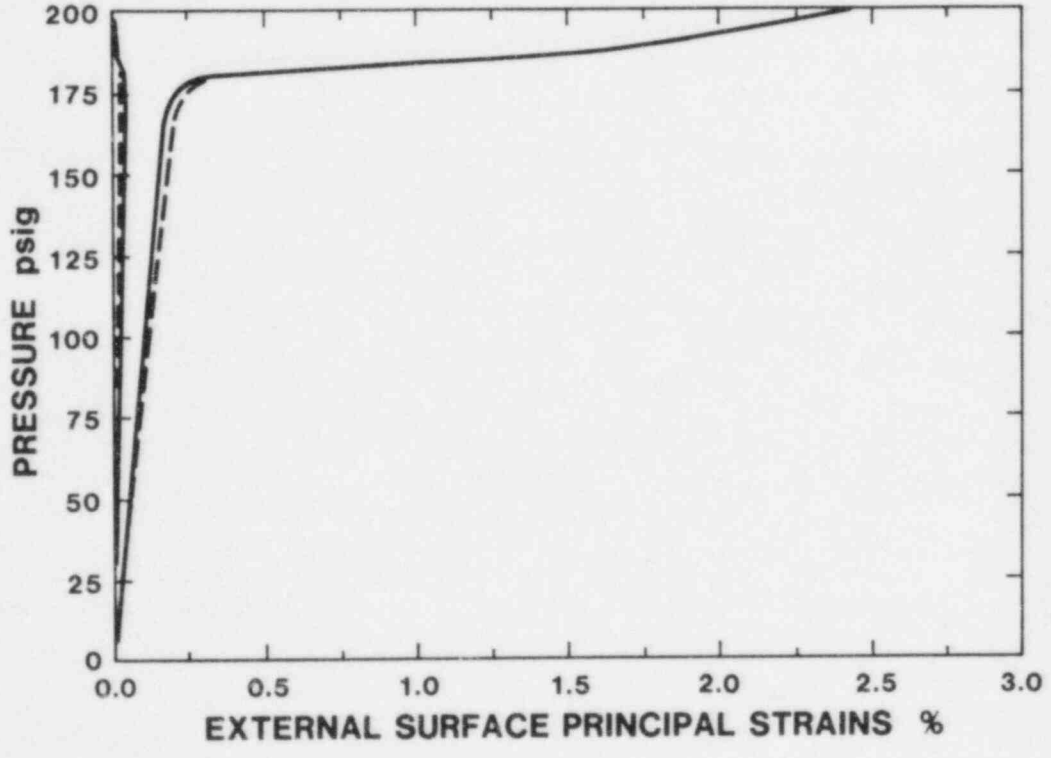

Figure 34 Comparison of CPM and PIM Strain in Cylinder 33" Above SF1

8. CLOSURE

Pretest predictions for the response of a 1:8-scale steel model of a containment building were made based on finite element methods. The design pressure of the model was 40 psig. Initial yielding occurred in areas characterized by bending, but strains did not increase rapidly until after membrane yielding of the cylinder began. The predicted membrane yield pressure was 180 psig. The equipment hatch sleeve is expected to deform into an oval shape, resulting in significant leakage by 210 psig. At this pressure, the maximum membrane strain in the cylinder wall should be 3.5%, with some bending strains as large as 9%.

9. REFERENCES

[1] HORSCHEL, D. S., "The Design, Fabrication, Testing and Analyses of Four 1:32-Scale Steel Containment Models," NUREG/CR-3902, SAND84-2153 (March 1985).

[2] VON RIESEMANN, W. A., et al., "U.S. NRC Containment Integrity Programs," Proceedings 8th Intl. Conf. on Structural Mechanics in Reactor Technology, Brussels, Belgium, August 19-23, 1985, Paper J 1/2.

[3] BLEJWAS, T. E., "Internal Pressure Experiments with Steel and Concrete Containment Models," Proceedings 8th Intl. Conf. on Structural Mechanics in Reactor Technology, Brussels, Belgium, August 19-23, 1985, Paper J 2/3.

[4] KOENIG, L. W., "Techniques and Results from the Internal Pressurization of a 1:8-Scale Steel Containment Model," Proceedings 8th Intl. Conf. on Structural Mechanics in Reactor Technology, Brussels, Belgium, August 19-23, 1985, Paper J 2/4.

[5] CLAUSS, D. B., and HORSCHEL, D. S., "Comparisons of Analytical and Experimental Results from Pressurization of a 1:8-Scale Steel Containment Model," Proceedings 8th Intl. Conf. on Structural Mechanics in Reactor Technology, Brussels, Belgium, August 19-23, 1985, Paper J 2/5.

[6] CLAUSS, D. B., "Comparison of Analytical Predictions and Experimental Results for a 1:8-Scale Steel Containment Model Pressurized to Failure," NUREG/CR-4209, SAND85-0679 (to be published).

[7] REESE, R. T. and HORSCHEL, D. S., "Design and Fabrication of a 1:8-Scale Steel Containment Model," NUREG/CR-3647, SAND84-0048 (February 1985).

[8] MARC General Purpose Finite Element Program, Revision K.1, MARC Analysis Research Corp., Palo Alto, California, 1983.

[9] PATRAN-G Interactive Pre and Post Processing, PDA Engineering, Irvine, California, 1980.

[10] CLAUSS, D. B., "Analysis of a 1:8-Scale Steel Containment Model Subject to Static, Internal Pressurization," Proceedings of the 2nd Workshop on Containment Integrity, June 13-15, 1984, NUREG/CR-0056, SAND84-1514 (August 1984).

[11] HORSCHEL, D. S. and CLAUSS, D. B., "The Response of Steel Containment Models to Internal Pressurization," Structural Engineering in Nuclear Facilities, Vol. 1, J.J. Ucciferro, editor, Proceedings of the Conference sponsored by the Committee on Nuclear Structures and Materials of the Structural Division of the ASCE, North Carolina State University, 1984.

[12] GOLLER, B., KRIEG, R., MESSEMER, G., "Behavior of Spherical PWR Containments Close to Reinforced Sections Under Excessive Internal Pressure," Proceedings of the 2nd Workshop on Containment Integrity, June 13-15, 1984, NUREG/CR-0056, SAND84-1514 (August 1984).

[13] NAGTEGAAL, J. C., and SLATER, J. G, "A Simple Noncompatible Thin Shell Element Based on Discrete Kirchoff Theory," presented at the ASME Winter Annual Meeting, Washington D.C., November 1981.

DISTRIBUTION

U.S. Government Printing Office
Receiving Branch Attn: NRC Stock
8610 Cherry Lane
Laurel, MD 20707
385 Copies for R1 and RD

US Nuclear Regulatory Commission
Division of Engineering Technology
5650 Nicholson Lane
Rockville, MD 20852
Attn: James Costello (5 copies)

Iowa State University
Department of Civil Engineering
420 Town Engineering Bldg.
Ames, IA 50011
Attn: L. Greimann

TVA
400 Commerce Avenue
Knoxville, TN 37902
Attn: D. Denton, W9A18

Los Alamos National Laboratories
PO Box 1663
Mail Stop N576
Los Alamos, NM 87545
Attn: C. Anderson

University of Illinois
Dept. of Civil Engineering
Urbana, IL 61801
Attn: C. Siess

University of Alberta
Dept. of Civil Engineering
Edmonton, Alberta, CANADA T6G 2G7
Attn: D. W. Murray

EBASCO Services, Inc.
Two World Trade Center
New York, NY 10048
Attn: J. J. Healdy, Consulting Engr.

Kernforschungszentrum Karlsruhe GmbH
Postfach 3640
D-7500 Karlsruhe
FEDERAL REPUBLIC OF GERMANY
Attn: R. Krieg, P. Gast (2 copies)

HM Nuclear Installation Inspectorate
Thames House North
Millbank, London, SW1
UNITED KINGDOM
Attn: R. J. Stubbs, T. Currie (2 copies)

Mr. Thomas J. Ahl
Nuclear Design Group
Chicago Bridge & Iron Co.
800 Jorie Boulevard
Oak Brook, IL 60521

P. A. Cox
Southwest Research Institute
6220 Culebra Road
PO Drawer 28510
San Antonio, TX 78284

William C. Black
2650 Woodside Road
Bethlemem, PA 18017

Ted M. Brown
Wiss, Janney, Elstner Assoc., Inc.
330 Pfingsten Road
Northbrook, IL 60062

Richard Denning
Battelle Columbus Laboratories
505 King Avenue
Columbus, OH 43201

Asadour H. Hadjian
Bechtel Power Corporation
12400 E. Imperial Highway
Norwalk, CA 90650

T. E. Johnson
Bechtel Power Corporation
777 East Eisenhower Pwy.
Ann Arbor, MI 48101

Bechtel Power Corporation
15740 Shady Grove Road
Gaithersburg, MD 20760
Attn: K. Y. Lee

Professor Mete A. Sozen
Dept. of Civil Engineering
University of Illinois
503 W. Michigan
Urbana, IL 61801

University of Tokyo
Institute of Industrial Science
22-1, Roppongi 7
Minatu-ku
Tokyo
JAPAN
Attn: H. Shibata

Argonne National Laboratory
9700 South Cass Avenue
Argonne, IL 60439
Attn: T. R. Bump, B. J. Hsieh,
M. H. Shackelford, S. H. Fistedis,
J. M. Kennedy, R. F. Kulak
R. W. Seidensticker,
G. A. McLennan (8 copies)

Dr. O. Mercier
EIR (Swiss Federal Institute for
Reactor Research)
CH-5303 Wuerlingen
Switzerland

Prof. Dr. H. Karwat
Lehrstuhl fuer Reakordynamik
und Reaktorsicherheit
Technische Universitaet Muenchen
D-8046 Garching
Federal Republic of Germany

Prof. Dr.-Ing. K. F. Kussmaul
Staatliche Materiapruefungsanstalt (MPA)
University of Stuttgart
Pfaffenwaldring 32
D-7000 Stuttgart 80
Federal Republic of Germany

Gesellschaft fuer Reaktorsicherheit (GRS)
Schwertnergasse 1
D-5000 Cologne 1
Federal Republic of Germany
Attn: H. Schulz, A. Hoefler (2 copies)

S. Chakraborty
Swiss Federal Nuclear Safety Inspectorate
Federal Office of Energy
CH-5303 Wuerenlingen
Switzerland

Dr. Wilfred E. Baker
Dept. of Ballistics & Exp. Sci.
Southwest Research Institute
6220 Culebra Road
PO Drawer 28510
San Antonio, TX 78284

W. R. Conley
David Taylor Naval Ship R&D Center
Code 1750.2
Bethesda, Maryland 20084

Sandia Distribution:
1510 J. W. Nunziato
1520 D. J. McCloskey
1523 J. H. Biffle
1523 D. B. Clauss (5)
1523 C. H. Conley
1524 J. Jung
1530 L. W. Davison
1540 W. C. Luth
1833 G. A. Knorovsky
3141 C. M. Ostrander (5)
3151 W. L. Garner
6241 D. L. Goodwin
6400 A. W. Snyder
6410 J. W. Hickman
6420 J. Walker
6440 D. A. Dahlgren
6442 W. A. Von Riesemann (10)
6442 R. N. Eyers
6442 D. S. Horschel
6442 L. N. Koenig
6442 D. L. Lambert
6442 P. E. Matson
6442 T. D. Molina
6444 L. D. Buxton
6446 L. L. Bonzon
6447 D. L. Berry
6449 K. D. Bergeron
7485 P. C. McKey
7485 F. H. Gallagos
7485 D. Leyva
7541 R. T. Reese
8024 M. A. Pound

Dr. John D. Stevenson
Stevenson & Associates
9217 Midwest Avenue
Cleveland, OH 44122

Technology for Energy Corporation
One Energy Center
Pellissippi Parkway
Knoxville, TN 37922
Attn: E. P. Stroupe

EG&G Idaho
Willow Creek Bldg. W-3
PO Box 1625
Idaho Falls, ID 83415
Attn: B. Barnes, T. L. Bridges,
J. A. Hunter (3 copies)

EG&G
Energy Measurements Group
Kirtland Operations
PO Box 4339, Station A
Albuquerque, NM 87196
Attn: W. Chaney

Sargent & Lundy Engineers
55 E. Monroe Street
Chicago, IL 60603
Attn: A. Walser

General Electric Company
175 Curtner Avenue
San Jose, CA 95125
Attn: J. E. Love, E. O. Swain,
D. K. Henrie (3 copies)

R. F. Reedy, Inc.
236 N Santa Cruz Avenue
Los Gatos, CA 95030

US Department of Energy
Office of Nuclear Energy
Mail Stop B-107
NE-540
Washington, DC 20545
Attn: A. Millunzi

Quadrex Corporation
1700 Dell Avenue
Campbell, CA 95008
Attn: Quazi A. Hossain

Chiapetta, Welch & Associates, Ltd.
9748 Roberts Road
Palos Hills, IL 60465
Attn: R. L. Chiapetta

ANATECH International Corporation
3344 N. Torrey Pines Court
Suite 320
LaJolla, CA 92037
Attn: Y. R. Rashid

Dr. Steve Hodge
Oak Ridge National Laboratories
Building 9108
PO Box Y
Oak Ridge, TN 37830

Dr. Trevor Pratt
Building 130
Brookhaven National Laboratory
Upton, NY 11973

Dr. Joseph J. Ucciferro
Structural Analysis Group
United Engineers & Constructors, Inc.
30 S. 17th Street
Philadelphia, PA 19101

Electrical Power Research Institute
3412 Hillview Avenue, PO Box 10412
Palo Alto, CA 94304
Attn: Dr. H. T. Tang, Dr. Y. K. Tang,
D. Winkleblack, Dr. Ian Wall,
J. J. Taylor (5 copies)

Commissariat a L'Energie Atomique (CEA)
Centre d'Etudes Nucleaires de Saclay
F-91191 Gif-Sur-Yyette Cedex
France
Attn: M. Livolant, P. Jamet (2 copies)

Professor Richard N. White
School of Civil & Environ. Engr.
Hollister Hall Cornell University
Ithaca, NY 14853

Motor-COLUMBUS Consulting Engineers, Inc.
Parkstrasse 27
CH-5401 Baden
SWITZERLAND
Attn: K. Gahler, A. Schopfer,
J. Jemielewski (3 copies)